# The Polar Express

Dynamic Aggregation under Policy Holonomy

*Online Appendix*

Chae-Yeon Xon

Yonsei University

September 2026

**Abstract**

This appendix contains proofs, inference details, numerical calculations, the Express data construction, and the constructed marketplace benchmark used in the paper.

*JEL Codes:* C14, C32, C61, C93, D12, E47, L91

*Keywords:* dynamic aggregation, holonomy, policy experiments, inverse design, Gorman aggregation, heterogeneous agents, delivery operations

Yonsei University. Email: eunixon@yonsei.ac.kr. This draft is circulated for discussion; comments and suggestions are welcome.

# Contents

# Appendix A. Policy lifts and holonomy

## A.1. Proof of proposition 2

Work in orthonormal frames for the Euclidean policy space and the phase metric at $x$. Let $A = A_s$, $R = R_s$, $C = AR^{-1}A'$, and $e = \nu - d_x \in \operatorname{im} A$. Positive definiteness of $R$ gives

$$\operatorname{im} C = \operatorname{im}(AR^{-1/2}) = \operatorname{im} A. \tag{A1}$$

The Moore–Penrose projector $CC^\dagger$ is the identity on this range. Hence the candidate $u^E = R^{-1}A'C^\dagger e$ is feasible because

$$Au^E = CC^\dagger e = e. \tag{A2}$$

Every feasible $u$ can be written as $u = u^E + z$ with $Az = 0$. The cross term in the objective vanishes:

$$z'Ru^E = z'A'C^\dagger e = (Az)'C^\dagger e = 0. \tag{A3}$$

Therefore

$$\frac{1}{2}u'Ru = \frac{1}{2}(u^E)'Ru^E + \frac{1}{2}z'Rz. \tag{A4}$$

Positive definiteness of $R$ gives the stated minimizer and its uniqueness. For $e \in \mathcal{E}_x$, substitution into the relative state lift gives

$$Dq_s L_s^E e = A_s R_s^{-1} A_s' C_s^\dagger e = e. \tag{A5}$$

Thus $L_s^E$ is injective and $\dim \operatorname{im} L_s^E = \rho$. If $L_s^E e \in \ker Dq_s$, equation (A5) gives $e = 0$, so $\operatorname{im} L_s^E \cap \ker Dq_s = \{0\}$. For any $z \in Dq_s^{-1}(\mathcal{E}_x)$, set $e = Dq_s z$. Then $z - L_s^E e \in \ker Dq_s$, which proves the decomposition in (10). A constant-rank matrix family has a smooth Moore–Penrose inverse, so $s \mapsto \operatorname{im} L_s^E$ is smooth. If $\mathcal{E}$ is involutive, each integral leaf has tangent bundle $\mathcal{E}$ and the decomposition is an Ehresmann connection on the restricted bundle. The case $\rho = m$ gives $\mathcal{E} = T\mathcal{X}$ and makes $C$ positive definite, so $C^\dagger = C^{-1}$.

## A.2. Horizontal path identity

Let $s_t$ solve (12). The chain rule and (A5) give

$$\frac{d}{dt}q(s_t) = d_{\gamma(t)} + Dq_{s_t} L_{s_t}^E\big(\dot\gamma_t - d_{\gamma(t)}\big) = \dot\gamma_t. \tag{A6}$$

The initial condition $q(s_0) = \gamma(0)$ then yields $q(s_t) = \gamma(t)$. Local existence and uniqueness follow from the ordinary differential equation theorem on a coordinate neighborhood. A closed $\gamma$ therefore maps its horizontal endpoint into the same fiber.

When $d \in \mathcal{E}$, equation (11) follows from $Dq_s(f_s - L_s^E d_x) = d_x - d_x = 0$. Substituting this decomposition into (12) gives

$$\dot{s}_t = L_{s_t}^E \dot{\gamma}_t + b_{s_t}. \tag{A7}$$

Thus the spatial flow-commutator calculation used in theorem 1 applies on the stated $b = 0$ neighborhood. For $b \neq 0$, equation (A7) defines a duration-dependent finite fiber transport. The finite-loop holonomy and polar recursion retain this transport, while a local curvature experiment requires drift compensation or a separate baseline-relative expansion.

### A.3. Proof of proposition A3

Write $J = D_U \Phi_T(U_0; s_0)$, $R = \mathsf{R}_T$, and $b = \gamma - \Phi_T(U_0; s_0)$. On $b \in \operatorname{im} J$, the same weighted projection argument as in equations (A1)–(A4) gives $J \Delta U^H = b$ and shows that every other linearized solution equals $\Delta U^H + z$ for $z \in \ker J$, with

$$\frac{1}{2}(\Delta U^H + z)' R (\Delta U^H + z) = \frac{1}{2}(\Delta U^H)' R \Delta U^H + \frac{1}{2} z' R z. \tag{A8}$$

This proves the minimum-cost claim. If $\operatorname{rank} J = mT$, the constant-rank level-set theorem makes $\Phi_T^{-1}(\gamma)$ a local embedded submanifold of dimension $kT - mT$. The matrix $JR^{-1}J'$ is positive definite, so the Newton correction varies continuously near $U_0$. If $\operatorname{rank} J = \rho_T < mT$, the product $JR^{-1}J'(JR^{-1}J')^\dagger$ is the orthogonal projector onto $\operatorname{im} J$. Hence $J\Delta U^H$ equals the attainable projection of $b$, and the remaining component is orthogonal to that range.

### A.4. Proof of proposition 3

If $\tau$ is constant on $\mathcal{O}_s^{\mathrm{Hol},E}$, its differential annihilates every tangent vector to that orbit. Conversely, a connected smooth manifold is path connected. For any $z_0, z_1 \in \mathcal{O}_s^{\mathrm{Hol},E}$, choose a piecewise $C^1$ curve $c : [0,1] \to \mathcal{O}_s^{\mathrm{Hol},E}$ joining them. Condition (14) gives

$$\tau(z_1) - \tau(z_0) = \int_0^1 D\tau_{c(t)} \dot{c}(t)\, dt = 0. \tag{A9}$$

Hence $\tau$ is constant on the orbit. If the orbit equals the fiber component, the same statement applies to that component. Under the spanning condition in the proposition, every orbit tangent vector is a linear combination of parallel transports of curvature values. Linearity of $D\tau$ makes annihilation of the spanning family equivalent to (14). The spanning statement is the role played by the curvature-generation theorem for holonomy (Ambrose and Singer 1953); the proposition states it as a condition so that the result also covers the Ehresmann setting used here.

### A.5. Proof of proposition A4

The parameterized ordinary differential equation theorem gives continuous differentiability of $S_t^\eta$ in $\eta$ on the common compact regularity neighborhood. Differentiate equation (A84) with respect to $\eta$. The chain rule gives equation (A85) and its initial condition. Applying the chain rule to $\tau^\eta(S_1^\eta) - \tau^\eta(s_\eta^\circ)$ gives the four terms in equation (A86). For the fixed-state curvature identity, differentiate the bilinear composition $D_s\tau^\eta\Omega^\eta(v, w)$ at fixed $(s, v, w)$ and apply the product rule. Conditional application to a stochastic innovation path follows path by path; dominated differentiation or uniform integrability permits integration over the prespecified innovation law.

### A.6. Proof of proposition 1

Write the flows of $H_1$ and $H_2$ as

$$X_a(x, y, h) = (x + a, y, h), \qquad Y_b(x, y, h) = (x, y + b, h + xb). \tag{A10}$$

Applying $X_a, Y_b, X_{-a}, Y_{-b}$ in that order gives

$$\begin{aligned}(x, y, h) &\mapsto (x + a, y, h) \mapsto (x + a, y + b, h + (x + a)b) \\ &\mapsto (x, y + b, h + (x + a)b) \mapsto (x, y, h + ab).\end{aligned} \tag{A11}$$

Interchanging the two initial directions gives $h - ab$. Applying $\tau(x, y, h) = h\ell$ proves (4). The additive correction gives terminal target $h + ab + c$, so $c = -ab$ is the unique scalar solution. Composition with the opposite orientation adds $ab - ab = 0$.

## Appendix B. Small-loop expansions

### B.1. A flow-commutator lemma

Let $X$ and $Y$ be $C^3$ vector fields on an open subset of $\mathbb{R}^n$, and let $\Phi_X^t$ and $\Phi_Y^t$ denote their local flows. Define

$$\mathcal{C}_\varepsilon^+ = \Phi_{-Y}^\varepsilon \circ \Phi_{-X}^\varepsilon \circ \Phi_Y^\varepsilon \circ \Phi_X^\varepsilon, \tag{A12}$$

$$\mathcal{C}_\varepsilon^- = \Phi_{-X}^\varepsilon \circ \Phi_{-Y}^\varepsilon \circ \Phi_X^\varepsilon \circ \Phi_Y^\varepsilon. \tag{A13}$$

LEMMA A1 (Flow commutator). *Uniformly on a compact coordinate neighborhood on which the flows exist,*

$$\mathcal{C}_\varepsilon^+(z) = z + \varepsilon^2[X, Y](z) + O(\varepsilon^3), \qquad \mathcal{C}_\varepsilon^-(z) = z - \varepsilon^2[X, Y](z) + O(\varepsilon^3). \tag{A14}$$

PROOF. The time-$\varepsilon$ flow expansion is

$$\Phi_X^\varepsilon(z) = z + \varepsilon X(z) + \frac{\varepsilon^2}{2} DX(z)X(z) + O(\varepsilon^3). \tag{A15}$$

Apply (A15) successively to the four maps in (A12). Terms of order $\varepsilon$ cancel. The order-$\varepsilon^2$ term is

$$DY(z)X(z) - DX(z)Y(z) = [X, Y](z). \tag{A16}$$

The same calculation after exchanging $X$ and $Y$ gives the second expansion. Bounded third derivatives on the compact neighborhood give the uniform remainder. □

### B.2. Proof of theorem 1

Take commuting coordinate extensions of $v$ and $w$ on $\mathcal{X}$, and let $X = v^H$ and $Y = w^H$ be their horizontal lifts. The horizontal-drift condition and equation (A7) make these fields the actual state velocities for the four report sides. Related-vector-field calculus gives

$$Dq_s[X, Y]_s = [v, w]_{q(s)} = 0. \tag{A17}$$

Thus $[X, Y]_s$ is vertical and equals $\Omega_s(v, w)$ under the sign convention in (15). Lemma A1 gives (17) and (18) in the chosen chart.

Taylor expansion of $\tau$ around $s$ gives

$$\begin{aligned} \tau(\mathcal{C}_\varepsilon^+(s)) &= \tau(s) + \varepsilon^2 D\tau_s\Omega_s(v, w) + O(\varepsilon^3), \\ \tau(\mathcal{C}_\varepsilon^-(s)) &= \tau(s) - \varepsilon^2 D\tau_s\Omega_s(v, w) + O(\varepsilon^3). \end{aligned} \tag{A18}$$

Subtracting and dividing by $2\varepsilon^2$ proves (19). Under $C^4$ smoothness the contrast has the expansion

$$\Delta(\varepsilon) = 2\varepsilon^2\kappa_\tau(s; v, w) + \varepsilon^3 c_3 + \varepsilon^4 c_4(\varepsilon), \tag{A19}$$

where $c_4(\varepsilon)$ remains bounded locally. Replacing $\varepsilon$ by $-\varepsilon$ preserves the quadratic term and reverses the cubic term. Adding the two expansions and dividing by $4\varepsilon^2$ proves (20).

The rectangle calculation extends to the homothetic loop used in the numerical section. Let $z = (z_1, z_2)$ be a fixed piecewise $C^2$ closed profile in the $(v, w)$ coordinate plane and set $\gamma_\varepsilon = x + \varepsilon z$. The second Picard iterate of the horizontal controlled equation has vertical part $\varepsilon^2 \mathcal{A}(z)\Omega_s(v, w)$, where $\mathcal{A}(z) = \frac{1}{2}\oint (z_1\, dz_2 - z_2\, dz_1)$ is signed area; the compact-neighborhood remainder is $O(\varepsilon^3)$. This follows by exchanging the order in the two iterated integrals and collecting their antisymmetric part into $[v^H, w^H]$. The central mirror replaces $\varepsilon$ by $-\varepsilon$, so the same fourth-order symmetrization applies. The loop in (A59) has signed area $o\pi r_a r_c s^2$, matching its reported normalization.

### B.3. Proof of corollary 1

If $\kappa_\tau(s; v, w) \neq 0$, equation (19) gives a nonzero target contrast for every sufficiently small $\varepsilon$ along a sequence, so $\tau$ varies on the local holonomy orbit. The sufficiency statement follows from proposition 3 and its spanning condition.

### B.4. Proof of proposition 4

Let $t \geq 0$ denote the common side scale of a commutator word of length $\ell_j$. The commutator expansion for smooth local flows gives an endpoint of the form $s + \sigma t^{\ell_j} Z_j(s) + O(t^{\ell_j+1})$, where $\sigma \in \{-1, 1\}$ records the orientation. The feasible phase-closing segment in the proposition changes the endpoint only at order $t^{\ell_j+1}$. Taylor expansion of $\tau$ therefore gives $\sigma t^{\ell_j} D\tau_s Z_j(s) + O(t^{\ell_j+1})$. Set $a_j = \sigma t^{\ell_j}$. Since $t = |a_j|^{1/\ell_j}$, this expression is equation (22). For a finite concatenation, the leading target displacement is $\sum_j a_j D\tau_s Z_j(s)$. The equation $b + \sum_j a_j D\tau_s Z_j(s) = 0$ has a solution exactly when $b$ belongs to the span of the displayed target words. Its range equals $\mathbb{R}^r$ exactly when that span has dimension $r$.

## Appendix C. Direction-reversal inference

### C.1. Population expansion

For an initial state $S = s$, theorem 1 yields

$$\text{(A20)} \qquad \frac{\Delta_s(\varepsilon) + \Delta_s(-\varepsilon)}{4\varepsilon^2} = \kappa_\tau(s; v, w) + r_s(\varepsilon), \qquad \sup_s \|r_s(\varepsilon)\| \leq C\varepsilon^2.$$

Equation (25) and randomization give the same initial-state law in every arm and identify each conditional contrast with its terminal-state target contrast. Taking expectations in (A20) proves (27).

### C.2. Proof of theorem 2

Let $a = (o, \sigma)$ index the four arms and assign the contrast signs $c_a = (1, -1, 1, -1)$. The triangular-array central limit theorem for the four independent arm means gives

$$\sqrt{n}\sum_a c_a(\overline{Y}_a - m_a) \implies \mathcal{N}\left(0, \sum_a \frac{\Sigma_a}{\pi_a}\right). \tag{A21}$$

Since

$$\sqrt{n}\varepsilon^2(\widehat{\kappa}_\varepsilon - \kappa_\varepsilon) = \frac{1}{4}\sqrt{n}\sum_a c_a(\overline{Y}_a - m_a), \tag{A22}$$

equation (28) follows. The sampling error has order $1/(\sqrt{n}\varepsilon^2)$, so $n\varepsilon^4 \to \infty$ gives consistency for $\kappa_\varepsilon$. The scaled smoothing bias is

$$\sqrt{n}\varepsilon^2(\kappa_\varepsilon - \mathbb{E}\kappa_\tau) = O(\sqrt{n}\varepsilon^4), \tag{A23}$$

which vanishes under the second rate condition. If $\varepsilon = n^{-a}$, the first condition is $a < 1/4$ and the second is $a > 1/8$.

### C.3. Proof of theorem 3

Random assignment and partial interference give $\mathbb{E}[\overline{Y}_c^p \mid A_c = a] = \mathbb{E}[\overline{Y}_c^p(a)] = m_a$. Linear combinations of the arm means therefore identify the orientation contrast and the four-arm contrast. Conditional on the realized arm count, independence across clusters gives

$$\operatorname{Var}(\overline{Y}_a) = \frac{1}{J_a}\operatorname{Var}\big(\overline{Y}_c^p(a)\big). \tag{A24}$$

Substitution of equation (29) proves equation (30). The multivariate independent-cluster central limit theorem applies to the stacked arm scores under the stated moment condition. Cross-arm score products vanish because each cluster occupies one arm and each arm score is centered. Multiplication by the finite-loop or $1/(4\varepsilon^2)$ contrast weights gives the asserted limits. Direct estimation of $\operatorname{Var}(\overline{Y}_c^p(a))$ treats the cluster mean as the observation and permits unrestricted dependence inside each cluster.

### C.4. Proof of theorem A1

Let $c_{o,\sigma} = (1, -1, 1, -1)$ follow the four-arm order in equation (26), and let $d_z$ equal one at $\eta_0 + \delta$ and minus one at $\eta_0 - \delta$. The estimator can be written

$$\widehat{\partial_\eta \kappa}_{\varepsilon,\delta} = \frac{1}{8\varepsilon^2\delta}\sum_{o,\sigma,z} c_{o,\sigma} d_z \overline{Y}_{o,\sigma,z}. \tag{A25}$$

The independent-arm triangular-array central limit theorem and the cell-share limits give a Gaussian limit for the centered sum with covariance $\sum_{o,\sigma,z} \Sigma_{o,\sigma,z}/\pi_{o,\sigma,z}$. Multiplication by 1/8 after scaling by $\sqrt{J}\varepsilon^2\delta$ proves equation (A91).

Taking expectations in equation (A25) and using equation (A90) gives the centered difference of $\kappa^{\eta}$, plus the centered differences of $\varepsilon^2 B(\eta)$ and $r_\varepsilon(\eta)$. Taylor's theorem with a bounded third derivative gives an $O(\delta^2)$ error for the first term. The mean-value theorem and the derivative bounds give $O(\varepsilon^2)$ and $O(\varepsilon^4)$ for the remaining terms. This proves the bias claim. Equation (A91) makes the sampling error $O_p((J\varepsilon^4\delta^2)^{-1/2})$, which vanishes under the consistency condition. Multiplication of the bias by $\sqrt{J}\varepsilon^2\delta$ gives the final centering condition. `PolicyTrajectoids_ShockComparativeStatics.v` checks the exact centered-difference error decomposition and the variance identity after division by $(2\delta)^2$.

### C.5. Proof of theorem A2

Within each matched set, random assignment maps the four potential cluster probe means into the four cells in equation (A92). The expectation of $D_b(\varepsilon)$ is therefore the set-level randomized four-arm contrast. Dependence among its four terms is retained inside the scalar or vector observation $D_b(\varepsilon)$. Independence across sets and the stated moment condition give the iid central limit theorem,

$$\sqrt{B}\left(B^{-1}\sum_{b=1}^{B} D_b - \mathbb{E}D_b\right) \Longrightarrow \mathcal{N}(0, \operatorname{Var}[D_b]). \tag{A26}$$

Consistency of the sample covariance of $D_b$ gives the standard-error statement. Under the sharp randomization null, permuting labels within each set reproduces the assignment distribution while retaining the observed outcomes and their within-set dependence.

### C.6. Loop-size balance

Let the leading bias be $B\varepsilon^2$ and the leading variance be $W/(n\varepsilon^4)$, where $B \neq 0$ and $W > 0$. The leading mean squared error is

$$B^2\varepsilon^4 + \frac{W}{n\varepsilon^4}. \tag{A27}$$

Differentiation in $x = \varepsilon^4$ gives $B^2 - W/(nx^2) = 0$, so $\varepsilon^8 = W/(nB^2)$. Hence $\varepsilon \asymp n^{-1/8}$ and the root mean squared error is of order $n^{-1/4}$.

### C.7. Proof of theorem 4

For one Gaussian observation in arm $a$, the two means differ by $s_a\varepsilon^2(\kappa_1 - \kappa_0)$ and the common variance is $\sigma_a^2$. The Gaussian divergence is the squared mean difference divided by $2\sigma_a^2$. Additivity over independent observations and $s_a^2 = 1$ give equation (32). For any rejection event $\phi$, $P_{\kappa_1}(\phi) \le P_{\kappa_0}(\phi) + \|P_{\kappa_1} - P_{\kappa_0}\|_{\mathrm{TV}}$. Pinsker's inequality and equation (32) give

$$\|P_{\kappa_1} - P_{\kappa_0}\|_{\mathrm{TV}} \le \sqrt{\frac{1}{2}\,\mathrm{KL}(P_{\kappa_0}, P_{\kappa_1})} = \frac{|\kappa_1 - \kappa_0|\varepsilon^2}{2}\left(\sum_a \frac{n_a}{\sigma_a^2}\right)^{1/2}. \tag{A28}$$

A level-$\alpha$ test has $P_{\kappa_0}(\phi) \le \alpha$, which proves (33). Stable allocations and variances make the right side beyond $\alpha$ converge to zero under the stated detection-boundary sequence. For the Wald statistic, the alternative shifts the standard normal limit by $\sqrt{n}\varepsilon^2\kappa/\sqrt{V}$. Setting the absolute noncentrality to $z_{1-\alpha/2} + z_{1-\beta}$ and solving for the continuous value of $n$ gives (34). At this value the rejection tail in the direction of $\kappa$ has probability $1 - \beta$ and the other rejection tail has nonnegative probability. Taking the next integer weakly increases the absolute noncentrality, which proves the planning statement.

### C.8. Proof of proposition 5

Weyl's singular-value inequality gives

$$|\widehat{\sigma}_j - \sigma_j(K)| \le \|\widehat{K} - K\|_{\mathrm{op}} \le \rho_n. \tag{A29}$$

If $\widehat{\sigma}_r > \rho_n$, equation (A29) gives $\sigma_r(K) > 0$ and the stated lower bound. On the confidence event, $K$ itself belongs to the operator ball defining (36), so $\mathrm{rank}(K) \in \mathcal{R}_n$. Taking probabilities proves the coverage statement.

## Appendix D. Area reachability and the curvature bridge

### D.1. Proof of proposition 6

If $b + aK_s = 0$, then $b = (-a)K_s \in \mathrm{row}(K_s)$. If $b \in \mathrm{row}(K_s)$, the Moore–Penrose inverse satisfies $bK_s^{\dagger}K_s = b$, and $a^\star = -bK_s^{\dagger}$ solves the closure equation. The Moore–Penrose solution lies in $(\ker_{\mathrm{L}}(K_s))^{\perp}$ and has the smallest Euclidean norm among all solutions, where $\ker_{\mathrm{L}}(K_s) = \{a : aK_s = 0\}$. Every solution $a$ satisfies $(a - a^\star)K_s = 0$, giving the affine set (39).

Under $\mathrm{rank}(K_s) = r$, rank–nullity for the map $a \mapsto aK_s$ gives $\dim\ker_{\mathrm{L}}(K_s) = L - r$, hence codimension $r$. Since $\mathrm{rank}(K_s) \le L = \binom{\rho}{2}$, full target rank implies the first inequality in (40). Solving $\rho(\rho-1)/2 \ge r$ for the positive root gives $\rho \ge (1 + \sqrt{1+8r})/2$, and integer $\rho$

gives the ceiling formula. The inequality $\rho \le m$ gives the second phase-area bound.

For a loop library $a = \eta P$, the closure derivative is $PK_s \in \mathbb{R}^{p\times r}$, whose rank is bounded by $p$. Thus full target rank requires $p \ge r$. Suppose $K_s$ has rank $r$. Choose a left inverse $K_s^\dagger \in \mathbb{R}^{r\times L}$ and construct a matrix $P_0$ whose first $r$ rows equal $K_s^\dagger$ and whose remaining rows are zero. Then $P_0K_s$ contains $I_r$ and has rank $r$. At least one $r \times r$ minor of $PK_s$ is therefore a nonzero polynomial in the entries of $P$. Its nonvanishing set is open and dense, which proves the final statement.

### D.2. Proof of proposition 7

The rank-$d$ matrix stratum $\Sigma_d \subset \mathbb{R}^{L\times r}$ is a smooth manifold of dimension

$$d(L + r - d). \tag{A30}$$

One way to obtain this count is to write a rank-$d$ matrix locally as $UV'$ with $U \in \mathbb{R}^{L\times d}$ and $V \in \mathbb{R}^{r\times d}$ of full column rank, then subtract the $d^2$-dimensional change of basis $(U, V) \mapsto (UG, VG^{-T})$. Its codimension in $\mathbb{R}^{Lr}$ is

$$Lr - d(L + r - d) = (L - d)(r - d). \tag{A31}$$

The preimage theorem for transverse maps gives the same codimension for $\mathcal{K}^{-1}(\Sigma_d)$ (Hirsch 1976). For $d < r$ this codimension is positive. In each coordinate chart a positive-codimension embedded submanifold has Lebesgue measure zero, so the finite union of lower-rank preimages has empty interior. The rank-deficient set is closed because it is defined by the vanishing of all $r \times r$ minors. Its complement is open and dense. When $L < r$, the row bound gives $\operatorname{rank}(K) \le L$ for every $K$.

### D.3. Area-coordinate remainder

LEMMA A2 (Rectangle remainder in area coordinates). *Let the horizontal vector fields and target be $C^3$ on a compact neighborhood. Implement a scalar oriented area a in a fixed coordinate plane by a rectangle with side lengths $c_1\sqrt{|a|}$ and $c_2\sqrt{|a|}$, where $c_1c_2 = 1$, and orientation* $\operatorname{sign}(a)$. *Then*

$$\tau(\mathrm{Hol}_{\gamma_a}(s)) - \tau(s) = a\kappa_\tau(s; E) + O(|a|^{3/2}). \tag{A32}$$

*For a finite concatenation over L coordinate planes, equation* (42) *holds after shrinking the neighborhood.*

PROOF. Lemma A1 gives the bracket term as the product of the two side lengths and bounds the remaining flow terms by a constant times the cube of their sum. The product equals $a$ after orientation is included, while the cubic bound is $O(|a|^{3/2})$. In a concatenation, the sum of the individual remainders is bounded by $C\sum_j |a_j|^{3/2} \le C\|a\|^{3/2}$ after changing the norm constant. Cross terms between the order-$a_j$ endpoint displacements have order $\|a\|^2$, which is bounded by a multiple of $\|a\|^{3/2}$ on a unit neighborhood. □

### D.4. Proof of theorem 5

Full column rank gives $K_s^\dagger K_s = I_r$. Hence

$$b + a^\star K_s = b - bK_s^\dagger K_s = 0. \tag{A33}$$

Using (42) and $\|a^\star\| \le \|b\|\|K_s^\dagger\|$ yields

$$\|b + F_s(a^\star)\| = \|\mathcal{R}_s(a^\star)\| \le C\|K_s^\dagger\|^{3/2}\|b\|^{3/2}, \tag{A34}$$

which proves (43). The uniform bounds along the sequence give (44). When $M = 0$, non-negativity of the norm and (44) give $e_k = 0$ for every $k \ge 1$. Suppose $M > 0$ and set $z_k = M^2 e_k$. Multiplying the recurrence by $M^2$ gives

$$z_{k+1} \le z_k^{3/2}. \tag{A35}$$

Induction yields $z_k \le z_0^{(3/2)^k}$. Dividing by $M^2$ proves (45).

### D.5. Proof of proposition 8

Weyl's inequality gives $\sigma_r(K) \ge \widehat{\sigma}_r - \rho > 0$, so both matrices have target rank $r$, $\widehat{K}^\dagger \widehat{K} = I_r$, and $\|\widehat{K}^\dagger\| = \widehat{\sigma}_r^{-1}$. Therefore

$$b + \widehat{a}K = b - \widehat{b} + \widehat{a}(K - \widehat{K}), \tag{A36}$$

$$\|\widehat{a}\| \le \frac{\|\widehat{b}\|}{\widehat{\sigma}_r}. \tag{A37}$$

The triangle and operator-norm inequalities give (46). When $\widehat{a}$ lies in the remainder neighborhood, adding $\mathcal{R}_s(\widehat{a})$ and applying (42) gives (47).

## Appendix E. Target-sensitive measurements

### E.1. Proof of proposition 6

Take $z$ with $zO = 0$. Since the rows of $N_O$ span the observational null space, $z = cN_O$ for some row vector $c$. Thus

$$zD = cN_OD = cA \in \mathrm{row}(A) = \mathrm{row}(B). \tag{A38}$$

The defining property of $B^\dagger$ gives

$$(zM^\star)B = zDB^\dagger B = zD, \tag{A39}$$

which proves reconstruction. For a competing $d_M$-coordinate factorization,

$$d^\star = \mathrm{rank}(N_OD) = \mathrm{rank}((N_OM)C) \le \mathrm{rank}(N_OM) \le d_M. \tag{A40}$$

The constructed $M^\star$ has $d^\star$ columns and attains the lower bound.

### E.2. A bounded-moment confidence band

PROPOSITION A1 (Two-sample target-moment band). *Suppose* $(\mu_1 - \mu_0)O = 0$, $d^\star \ge 1$, $0 < \alpha < 1$, *and* $n_0, n_1 \ge 1$. *Let* $M_j(S) \in [\ell_j, u_j]$ *be the jth column weight of* $M^\star$. *Draw* $n_0$ *independent microstates from distribution* $\mu_0$ *and* $n_1$ *from* $\mu_1$, *and let* $\widehat{d}_j$ *be the difference of their sample mean weights. With probability at least* $1 - \alpha$ *simultaneously over* $j = 1, \ldots, d^\star$,

$$|\widehat{d}_j - (\mu_1 - \mu_0)M_j| \le (u_j - \ell_j)\sqrt{\frac{1}{2}\left(\frac{1}{n_0} + \frac{1}{n_1}\right)\log\frac{2d^\star}{\alpha}}. \tag{A41}$$

*Multiplying the coordinate half-width vector by* $|B|$ *gives a simultaneous coordinatewise band for* $(\mu_1 - \mu_0)D$.

PROOF. Hoeffding's inequality for the difference of two bounded sample means gives tail probability at most

$$2\exp\left\{-\frac{2t^2}{(u_j - \ell_j)^2(1/n_0 + 1/n_1)}\right\}. \tag{A42}$$

Set this expression equal to $\alpha/d^\star$ and apply the union bound. Equation (51) transfers the moment difference through $B$; the triangle inequality gives the stated target band. □

## Appendix F. Polar aggregation and loop quotients

### F.1. Proof of proposition 9

For a phase loop based at $x$, both endpoints have phase report $x$. Substitution into (54) gives

$$\tau(\mathrm{Hol}_\gamma(s)) - \tau(s) = \alpha(x) + M(\mathrm{Hol}_\gamma(s))B(x) - \alpha(x) - M(s)B(x), \tag{A43}$$

which is (55). For a tangent vector $\xi \in T_s\mathcal{S}$, the chain and product rules give

$$D\tau_s\xi = D\alpha_x Dq_s\xi + (DM_s\xi)B(x) + M(s)DB_x Dq_s\xi. \tag{A44}$$

Curvature is vertical, so $Dq_s\Omega_s(v,w) = 0$. Setting $\xi = \Omega_s(v,w)$ in (A44) yields the first identity in (56). Stacking the area basis gives $K_s = K_{M,s}B(x)$. The matrix-product rank inequalities give

$$\mathrm{rank}(K_s) \leq \min\{\mathrm{rank}\,K_{M,s}, \mathrm{rank}\,B(x)\} \leq g. \tag{A45}$$

### F.2. Proof of theorem 7

Let $L = DM_s|_{V_s} : V_s \to \mathbb{R}^g$. The annihilator identity for a linear map on a finite-dimensional vector space is

$$(\ker L)^\circ = \mathrm{im}\,L^* = \mathrm{span}\{dM_{1,s}|_{V_s}, \ldots, dM_{g,s}|_{V_s}\}. \tag{A46}$$

Suppose (60) holds and take $\xi \in \ker L$. Every transported target covector in (58) belongs to $(\ker L)^\circ$, so $D(\tau \circ \mathrm{Hol}_\gamma)_s\xi = 0$ for each $\gamma \in \mathcal{L}_x$. This is (59).

Conversely, suppose (59) holds. Each scalar covector $D(\tau^a \circ \mathrm{Hol}_\gamma)_s|_{V_s}$ vanishes on $\ker L$. Equation (A46) places every such covector in $\mathrm{im}\,L^*$, and taking their span yields (60). Hence $d_G^{\mathrm{loc}}(s) \leq \mathrm{rank}\,L \leq g$. If the transported target span has an additive differential basis $(dM_{1,s}, \ldots, dM_{d,s})$, its span equals $\mathcal{W}^\star_{\tau,s}$ and the first part gives sufficiency with $d = d_G^{\mathrm{loc}}(s)$. The lower bound gives minimality. Existence of an additive representation at the bound supplies such a basis after deleting linearly dependent coordinates, which gives the stated equivalence.

### F.3. Proof of corollary 2

Apply theorem 7 to the joint index set of environment–loop–target triples in equation (62). The annihilator argument is unchanged because every pulled-back response covector belongs to the common dual fiber $V_s^*$. Its span therefore gives the level lower bound and an additive differential frame gives attainment. If $\mathcal{I}_1 \subseteq \mathcal{I}_2$, every generator of $\mathcal{W}^\star_{\tau,\mathcal{I}_1,s}$ is also a generator of $\mathcal{W}^\star_{\tau,\mathcal{I}_2,s}$. Subspace inclusion and dimension monotonicity yield equation (65).

Shock-derivative robustness applies the same annihilator identity to the enlarged covector family consisting of every level covector indexed by $\mathcal{I}_0$ and the derivatives in equation (63). The minimum rank is therefore the dimension of their sum. Since $\mathcal{W}^\star_{\tau,\mathcal{I}_0,s}$ is a subspace of this sum, the inequality in equation (66) follows. Equality of the two finite dimensions holds exactly when every derivative covector already belongs to the prespecified-family level span. An additive differential frame for the sum gives attainment among additive measurements. If $\mathcal{I}_0$ contains an open neighborhood of $\eta_0$, $\Psi_{\eta,\gamma} = b_{\eta,\gamma} \circ (q, M)$ on that neighborhood, and $(\eta, s) \mapsto b_{\eta,\gamma}$ is $C^1$, differentiation gives $\partial_\eta \Psi_{\eta,\gamma} = (\partial_\eta b_{\eta,\gamma}) \circ (q, M)$ and hence jet closure. Along a moving baseline, the chain rule adds $D\Psi_{\eta,\gamma}\partial_\eta s^\circ_\eta$; level closure makes this term a function of $D(q, M)\partial_\eta s^\circ_\eta$. A finite collection of level restrictions leaves the shock derivative unrestricted. For example, $\Psi_\eta(z) = (\eta^2 - 1)z$ equals zero at both prespecified levels $\eta = -1$ and $\eta = 1$, while $\partial_\eta \Psi_\eta(z) = 2\eta z$ retains the omitted state coordinate at either level.

### F.4. Proof of proposition 10

Let $\Psi^{a_1}_{\gamma_1}, \ldots, \Psi^{a_d}_{\gamma_d}$ be the scalar response coordinates whose differentials form the frame in the theorem. Define

$$M^\star(s) = \left(\Psi^{a_1}_{\gamma_1}(s), \ldots, \Psi^{a_d}_{\gamma_d}(s)\right). \tag{A47}$$

Then $DM^\star$ has rank $d$. The constant-rank theorem supplies local coordinates $(y, z)$ with $y = M^\star(s)$. For every $\gamma$ and $a$, membership $D\Psi^a_\gamma(s) \in \mathcal{W}^\star_{\tau,s} = \operatorname{row} DM^\star_s$ makes every derivative of $\Psi^a_\gamma$ in a $z$ direction equal to zero. The assumed connectedness of each $z$ section lets integration along that section give a $C^1$ function $b^a_\gamma$ satisfying $\Psi^a_\gamma = b^a_\gamma \circ M^\star$. Stacking the target coordinates gives the decoder $b_\gamma$.

Each component of $M^\star$ is a response coordinate, so equation (67) implies equality of $M^\star$. The decoders give the converse implication. Hence the fibers of $M^\star$ are the local dynamic target equivalence classes. For generator $g_j$, the $\ell$th component of $M^\star \circ g_j$ equals $\tau^{a_\ell} \circ g_{\gamma_\ell} \circ g_j$, which is another word response. Its decoder through $M^\star$ supplies component $\ell$ of the induced update. Thus $M^\star$ is transport-closed.

Let $M$ be another dynamically target-sufficient $C^1$ representation with decoders $b_\gamma$. Differentiating $\Psi_\gamma = b_\gamma \circ M$ gives

$$D\Psi^a_\gamma(s) = Db^a_\gamma(M(s))DM_s. \tag{A48}$$

Therefore $\mathcal{W}^\star_{\tau,s} \subseteq \operatorname{row} DM_s$, and $d \leq \operatorname{rank} DM_s$. The constructed representation has rank and dimension $d$, which proves the claim.

## F.5. Proof of theorem A3

The equality $P_jH = H$ makes $\operatorname{col}(H)$ invariant under every $P_j$, so each $P_j$ induces $\overline{P}_j$ on the quotient. Suppose a $g$-coordinate polar quotient satisfies (A94). Passing both equations to the quotient gives

$$\pi(\operatorname{col} D) \subseteq \operatorname{span} \pi(\operatorname{col} W), \qquad \overline{P}_j \operatorname{span} \pi(\operatorname{col} W) \subseteq \operatorname{span} \pi(\operatorname{col} W). \tag{A49}$$

The defining minimality of (A96) therefore gives $\overline{\mathcal{V}}_\infty \subseteq \operatorname{span} \pi(\operatorname{col} W)$ and $d_G \leq g$.

For attainment, choose a basis of $\overline{\mathcal{V}}_\infty$, lift its $d_G$ elements to $\mathbb{K}^N$, and stack the lifts as the columns of $W$. Since $\pi(\operatorname{col} D)$ lies in $\overline{\mathcal{V}}_\infty$, each column of $D$ equals a linear combination of columns of $W$ plus an element of $\operatorname{col}(H)$. Hence $D = HC + WB$ for suitable $C$ and $B$.

$$\overline{P}_j \pi(W) = \pi(W) R_j, \qquad P_j W - W R_j = H A_j \tag{A50}$$

for suitable $R_j$ and $A_j$, where the second equality follows because the first difference has columns in $\operatorname{col}(H)$. These matrices satisfy (A94) with $g = d_G$.

The sequence in (A97) is increasing. Its union contains every finite word in (A96), and every stage lies in their span, so its stabilized value is $\overline{\mathcal{V}}_\infty$. Each strict enlargement raises dimension by at least one. The quotient has dimension $N - \operatorname{rank}(H)$, which gives the stated stopping bound.

Finally, multiply (A94) on the left by $\mu$. The target equation gives $\mu D = (\mu H)C + (\mu W)B$. The transition equation gives $(\mu P_j)W = (\mu H)A_j + (\mu W)R_j$. Since $(\mu P_j)H = \mu H$, both identities depend on the distribution through $m = \mu W$, proving (A95).

## F.6. Proof of corollary A1

The tangent space of a phase fiber is $\mathcal{T}_H = \{z \in \mathbb{K}^N : zH = 0\}$. For a loop word $\gamma = (j_1, \ldots, j_k)$, write $P_\gamma = P_{j_1} \cdots P_{j_k}$. The directional derivative of scalar target coordinate $c \in \mathbb{K}^r$ after this word is

$$z \longmapsto z P_\gamma D c, \qquad z \in \mathcal{T}_H. \tag{A51}$$

Two loading vectors define the same functional on $\mathcal{T}_H$ exactly when their difference belongs to $\operatorname{col}(H)$. Consequently the span of the word-response covectors on the fiber is isomorphic to

$$\operatorname{span}\left\{\pi(P_\gamma D c) : \gamma \in \mathcal{L}_x,\ c \in \mathbb{K}^r\right\} = \overline{\mathcal{V}}_\infty. \tag{A52}$$

Its dimension is $d_G$. The construction in theorem A3 lifts a basis of this space to $W$ and supplies the target decoder and affine updates in (A94). Its lower-bound argument applies to every linear additive representation closed under the same loop library, which proves the corollary.

### F.7. Proof of corollary A2

Write $h = h_x$. The recursion $m_{k+1} = hA + m_k R$ and $m_0 = m$ gives the formula in (A98) by induction. The induction step is

$$hA + \left( mR^k + hA \sum_{\ell=0}^{k-1} R^\ell \right) R = mR^{k+1} + hA \sum_{\ell=0}^{k} R^\ell. \tag{A53}$$

Phase preservation and the first identity in (A95) give $\tau(\mu P^k) - \tau(\mu) = (m_k - m_0)B$, which yields the target formula. Vanishing of this product is equivalent to membership of the bracketed row in the right kernel of $B$. Substitution of $R^k = I_g$ and $A \sum_{\ell=0}^{k-1} R^\ell = 0$ gives closure for every $m_0$.

### F.8. Proof of theorem A4

Apply the affine recursion $m_t = h_x A_{j_t} + m_{t-1} R_{j_t}$ successively. An induction on $T$ gives $m_T = m_0 R_{j_1} \cdots R_{j_T} + h_x \sum_{t=1}^{T} A_{j_t} R_{j_{t+1}} \cdots R_{j_T}$. Subtracting $m_0$ and multiplying by the target slope $B$ proves equations (A99)–(A100). For loop type $j$, the population normal equation conditional on that type is $\mathbb{E}[z'_{ij} m^+_{ij} \mid j] = Q_j \Theta_j$. Positive definiteness of $Q_j$ identifies $\Theta_j = Q_j^{-1} \mathbb{E}[z'_{ij} m^+_{ij} \mid j]$; the target regression identifies $(C', B')'$ by the same argument. Convergence of the sample second moments makes the sample normal-equation inverses converge to their population inverses. Independent-cluster sampling, the uniform $2 + \delta$ moment bound, cluster Lindeberg condition, positive limiting loop shares, covariance convergence, and fixed regressor dimension then give the joint cluster central limit theorem and the usual least-squares linear representations for these coefficient estimators, with coefficient influence covariance obtained by sandwiching $\Omega$ with the limiting inverse design matrices. Append the initial-moment influence terms supplied by the theorem's joint representation; fixed initial moments contribute zero. For a fixed word, equation (A100) is a polynomial in the coefficient matrices and a linear function of the initial moments. The multivariate delta method therefore gives equation (A102), with $J_\gamma$ equal to its derivative and $\Sigma$ equal to the covariance of the stacked influence function. If $W$ is estimated, substitute its assumed asymptotic linear expansion into $m = \mu W$ and append that influence term before applying the same delta method. In a cross-fitted implementation, the same step requires a foldwise influence representation and an aggregate remainder of order $o_p(n^{-1/2})$; orthogonality and nuisance-rate conditions can supply this representation for a chosen first-stage procedure.

## Appendix G. Heterogeneous-agent computation

### G.1. Household problem

The fixed-price calculation in this subsection uses household state $(a_i, y_j)$ on 36 asset nodes and three income nodes. Income follows the transition matrix

$$\Pi_y = \begin{bmatrix} 0.91 & 0.08 & 0.01 \\ 0.055 & 0.89 & 0.055 \\ 0.01 & 0.08 & 0.91 \end{bmatrix}. \tag{A54}$$

The asset grid is $18z^{2.2}$ for 36 equally spaced values of $z \in [0, 1]$. Preferences have discount factor 0.985, CRRA coefficient 2, and logit taste scale 0.035. For current microstate $i$ and asset choice $a'$, resources under policy $u = (u_r, u_w, u_y)$ are

$$c_i(a'; u) = (1 + r + 0.004u_r)a_i + y_i + 0.060u_w\psi_w(i) + 0.045u_y\psi_y(i) - a'. \tag{A55}$$

The tilts $\psi_w$ and $\psi_y$ are centered, variance-normalized asset and income scores, then scaled to unit maximum absolute value. The smoothed Bellman operator is

$$V_i = \chi \log \sum_{a' : c_i(a';u) > 0} \exp \left\{ \frac{U(c_i(a'; u)) + \beta\mathbb{E}[V(a', y') \mid y_i]}{\chi} \right\}. \tag{A56}$$

The associated choice probabilities and $\Pi_y$ form the $108 \times 108$ household transition matrix $P(u)$.

### G.2. Policy connection on the distribution simplex

The code solves the stationary household problem at $u = 0$ and forms centered derivatives

$$Q_j = \frac{P(he_j) - P(-he_j)}{2h}, \qquad h = 10^{-4}. \tag{A57}$$

The maximum absolute row-sum error across the three derivatives is $1.61 \times 10^{-12}$. For distribution $\mu$, stack the policy fields $g_j(\mu) = \mu Q_j$ as the rows of $G(\mu)$. With report-loading matrix $C = [a, c]$, the row-vector convention gives $A(\mu) = G(\mu)C \in \mathbb{R}^{3\times2}$, the transpose-coordinate representation of the map $A_s$ in (6). The implementation checks that $A(\mu)$ has column rank two at every integration evaluation. The implemented lift is

$$u^H(\mu, \nu) = \nu[A(\mu)'A(\mu)]^{-1}A(\mu)', \qquad \dot{\mu} = u^H(\mu, \nu)G(\mu). \tag{A58}$$

Multiplying (A58) by $C$ gives $\dot{\mu}C = \nu$. The ODE integrator therefore traces the requested asset–consumption path up to numerical tolerance.

The phase loops have the parametric form

$$\text{(A59)} \qquad \gamma_{o,s}(t) = x_0 + \left(osr_a \sin(2\pi t),\ sr_c[1 - \cos(2\pi t)]\right), \qquad r_a = 0.012, \quad r_c = 0.0035,$$

where $o \in \{-1, 1\}$ is orientation and $s$ can have either sign for the mirror operation. Their signed area is $o\pi r_a r_c s^2$. The probe is an interest-rate wedge of size $-0.75$ in normalized units, decaying at rate 0.72 over nine periods. Conditional consumption-response kernels at horizons 0, 3, and 7 form the columns of $D$.

### G.3. Numerical diagnostics

Table A1 gives the four-arm curvature sequence. Its stability under shrinking loop size is the numerical counterpart of equation (20). All values refer to the stated 108-state discretization.

TABLE A1. Shrinking-loop target curvature

| Loop scale | Area | Horizon 0 | Horizon 3 | Horizon 7 |
|---|---|---|---|---|
| 0.50 | $3.299 \times 10^{-5}$ | 0.002967 | 0.0003677 | −0.0002091 |
| 0.40 | $2.111 \times 10^{-5}$ | 0.002957 | 0.0003667 | −0.0002085 |
| 0.30 | $1.188 \times 10^{-5}$ | 0.002949 | 0.0003659 | −0.0002080 |
| 0.22 | $6.386 \times 10^{-6}$ | 0.002945 | 0.0003654 | −0.0002077 |
| 0.16 | $3.378 \times 10^{-6}$ | 0.002942 | 0.0003652 | −0.0002076 |

The baseline scalar defect is $9.58 \times 10^{-8}$. The oriented correction areas are $-3.246 \times 10^{-5}$, $-5.511 \times 10^{-6}$, $-4.077 \times 10^{-7}$, and $-9.301 \times 10^{-9}$. The resulting defects are $1.63 \times 10^{-8}$, $1.20 \times 10^{-9}$, $2.74 \times 10^{-11}$, and $1.72 \times 10^{-13}$. The largest phase-path error over the bridge loops is $1.70 \times 10^{-12}$.

The scalar measurement rank is one. For the three-horizon vector it is three, with

$$\text{(A60)} \quad (\sigma_1, \sigma_2, \sigma_3) = (0.1109169, 0.0100209, 0.0035317), \qquad v_1 = (0.9880, 0.1496, -0.0372).$$

The rank-one approximation associated with $v_1$ captures 0.9909 of the squared fiber-response norm, and the remaining operator norm is 0.0100. The curvature vector has relative residual 0.0422 after projection on that polar slope. Figure A1 displays the scalar weight and the four-arm sampling calculation. The 95 percent half-widths exceed the corresponding population curvatures by more than two orders of magnitude under 500,000 terminal draws per arm. Division by the small loop area produces this loss of precision, as equation (28) records. This calibration treats the four-arm exercise as a design diagnostic and supplies no finite-sample evidence for the curvature coordinates.

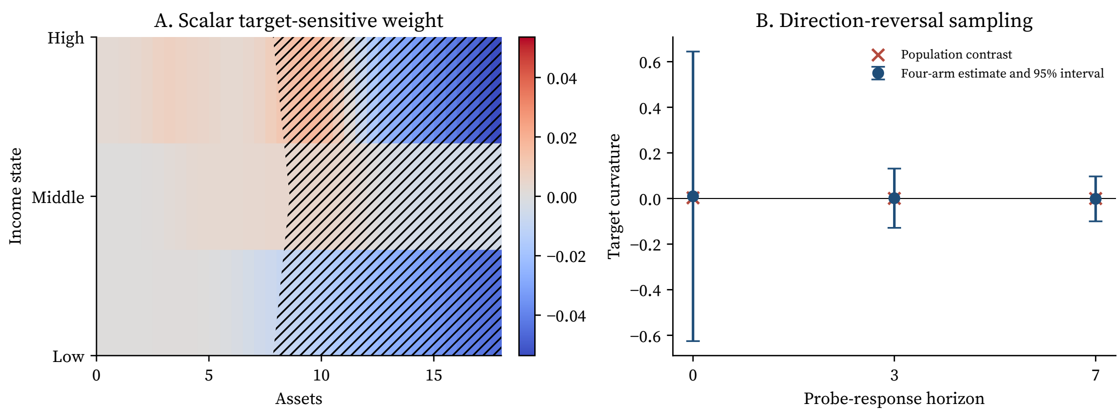


FIGURE A1. Target-sensitive weight and four-arm sampling variation

Panel A plots the horizon-0 probe-response kernel over assets and income states. The color scale is symmetric around zero, and hatching marks negative weights. Its sample average is the scalar target-sensitive measurement. Panel B gives the four-arm curvature estimate from 600 Monte Carlo replications with 500,000 terminal microstate draws in each arm. Bars are coordinatewise normal 95 percent intervals computed from arm variances. Their scale shows that the displayed design is statistically uninformative for the curvature coordinates.

### G.4. Production-economy feedback benchmark

The production-economy calculation uses 24 asset nodes on the same curved grid and the three-state income chain in (A54). Its distribution has 72 coordinates. Aggregate assets and labor determine prices through equation (70). The capital conversion factor is 18.4461446, productivity is 0.5749637, capital share is 0.36, and depreciation is 0.025. At the stationary distribution, aggregate assets are 0.896483, labor is 1.028947, production capital is 16.536654, output is 1.607730, the wage is one, the net return is one percent, and current consumption is 1.037912.

For a current distribution $\mu$ and policy coordinate $u$, the household kernel is $P(\mu, u)$ because wages and returns enter current resources. The continuation value used inside this one-period kernel equals its steady-state value. This specification separates current factor-price feedback and subsequent distributional propagation. The uncontrolled field and three policy fields are computed from

$$f(\mu) = \mu[P(\mu, 0) - I], \qquad g_j(\mu) = \mu \left. \frac{\partial P(\mu, u)}{\partial u_j} \right|_{u=0}, \tag{A61}$$

where centered differences use a policy step of $2 \times 10^{-4}$. Directional derivatives of the nonlinear report in (71) use a simplex step with Euclidean norm $2 \times 10^{-6}$. The partial lift solves the minimum-cost policy problem after subtracting the reported drift. The phase-policy map has rank two along every integrated path; its smallest singular value across the reported scales is 0.03060.

The requested phase curve is equation (72), traversed over 12 quarters. Adaptive integration uses relative tolerance $5 \times 10^{-8}$, absolute tolerance $2 \times 10^{-11}$, and a maximum step of one eighteenth of normalized path time. At scale 0.1, the maximum phase error is $7.13 \times 10^{-9}$ percentage point clockwise and $2.84 \times 10^{-9}$ counterclockwise. The corresponding maximum policy-coordinate norms are 2.39 and 1.99. The largest absolute coordinates across the three instruments are $(1.624, 1.450, 1.099)$ clockwise and $(1.020, 1.294, 1.155)$ counterclockwise.

The common probe begins with a return coordinate of $-1.5$, equivalent to a 60-basis-point cut under the return scale 0.004, and decays by 0.68 for eight quarters. Its consumption responses from the stationary distribution are $(-0.127736, -0.253944, -0.568246)$ percentage point at horizons 0, 3, and 7. The clockwise horizon-0 defects are $-0.00178$, $-0.00335$, $-0.00532$, and $-0.00688$ percentage point at scales 0.1, 0.2, 0.35, and 0.5; the counterclockwise defects are $-0.00343$, $-0.00674$, $-0.01144$, and $-0.01586$. The clockwise terminal-distribution distance rises from 0.00304 to 0.01497 in $\ell_1$ across these scales; the counterclockwise distance rises from 0.00798 to 0.03775.

The terminal-sampling calculation treats the horizon-0 conditional response kernel as a household weight. For the scale-0.5 clockwise–counterclockwise contrast, the normal approximation gives 27,194 independent household draws per orientation for a two-sided five-percent test with 80-percent power. Policy-path assignment occurs at the economy, jurisdiction, or market level. Letting $J_o$ denote independent clusters assigned to orientation $o$, cluster-level variation determines causal path precision, while household sampling within a cluster determines terminal target-measurement precision.

The polar library starts from the three conditional probe weights, squared assets, income interactions, and lower- and upper-tail indicators. Phase-known columns are projected out and the residual weighted covariance is normalized, leaving seven fiber coordinates. Sixteen Hadamard perturbations of asset and income scores, together with the stationary distribution, generate 17 initial episodes. For each orientation, least squares estimates the affine map from initial phase and fiber coordinates to terminal fiber coordinates. The clockwise and counterclockwise moment-law root mean squared errors are $9.10 \times 10^{-5}$ and $9.04 \times 10^{-5}$; the stacked episode regressor has condition number 207.7. A target regression on the same coordinates has root mean squared error $4.56 \times 10^{-4}$ percentage point and maximum error 0.00310 percentage point.

For the clockwise–counterclockwise word at scale 0.1, the estimated affine laws and direct propagation give

$$\begin{aligned} \widehat{h}^{\mathrm{cw,ccw}} &= (-0.003461, 0.000455, 0.004426), \\ h^{\mathrm{direct}} &= (-0.003737, 0.000551, 0.004821), \\ |\widehat{h}^{\mathrm{cw,ccw}} - h^{\mathrm{direct}}| &= (0.000276, 0.000096, 0.000395) \end{aligned} \tag{A62}$$

in percentage-point units. These records evaluate the finite-dimensional quotient over the 17-episode neighborhood. The cluster asymptotics in theorem A4 apply to repeated policy episodes, with the moment construction and coefficient estimation included in the stacked influence representation.

### G.5. Perfect-foresight transition equilibrium

The transition calculation uses the 24-asset, three-income production economy and solves household values backward over a 24-quarter loop-and-tail horizon. The last value equals the stationary continuation value. Given a distribution guess, wages and returns are computed from equation (70), period choice kernels are obtained by backward induction, and the distribution is propagated forward. Damped fixed-point iteration continues until the maximum distribution discrepancy is below $5 \times 10^{-9}$; the accepted consistency discrepancy is below $1.5 \times 10^{-8}$. A separate 20-quarter baseline-and-probe equilibrium evaluates the terminal distribution.

For a 12-quarter loop, the stacked control $U$ has 36 coordinates and the report path

$\Phi_{12}(U)$ has 24 coordinates. Starting from zero controls, the code computes $D\Phi_{12}$ by one-sided policy perturbations of $8 \times 10^{-4}$ and updates

$$U^{(j+1)} = U^{(j)} - D\Phi_{12}(U^{(j)})^{\dagger}\left[\Phi_{12}(U^{(j)}) - \gamma\right]. \tag{A63}$$

A line search and Broyden updates supply intermediate Jacobians; a full path Jacobian is recomputed at each reported solution. Every solution has rank 24. The smallest singular values over both orientations are 0.05068, 0.04894, 0.04559, and 0.03862 at scales 0.10, 0.25, 0.50, and 1.00. The maximum report errors are $5.67 \times 10^{-6}$, $4.46 \times 10^{-6}$, $7.50 \times 10^{-6}$, and $9.53 \times 10^{-6}$ percentage point.

The ordinary probe responses and the horizon-0 defects over the four loop scales are

$$\begin{aligned} \tau_0 &= (-0.118261, -0.393364, -0.441442), \\ h_0^{\mathrm{cw}} &= (0.000064, -0.000068, -0.000864, -0.004319), \\ h_0^{\mathrm{ccw}} &= (-0.000431, -0.001206, -0.002826, -0.007145) \end{aligned} \tag{A64}$$

in percentage-point units. At scale 0.1, the clockwise and counterclockwise terminal-distribution distances are 0.002242 and 0.003336 in $\ell_1$, while the end of the zero-policy tail lies 0.000400 and 0.000413 from the stationary distribution.

The seven-coordinate polar fit uses the three probe-response weights, asset and income powers and interactions, and distributional tail indicators after projecting out phase-known loadings. A stationary episode and 16 Hadamard tilts generate the estimation design at scale 0.1. The target regression root mean squared error is $4.76 \times 10^{-6}$ percentage point. The clockwise and counterclockwise moment-law root mean squared errors are $9.36 \times 10^{-5}$ and $1.05 \times 10^{-4}$, and the regressor condition number is 310.8. For a clockwise–counterclockwise composition, predicted and direct defect vectors are $(-0.000685, 0.000419, 0.000587)$ and $(-0.000452, 0.000302, 0.000409)$ percentage point. Their absolute errors are $(0.000233, 0.000118, 0.000177)$. This composition records finite-neighborhood misspecification of the seven-coordinate quotient. The current-value calculation above supplies a second quotient diagnostic.

## Appendix H. Express operational-state construction

### H.1. Proof of proposition 11

Conditional expectation minimizes mean squared loss over its information set, so the two infima in equation (75) are attained by $\mu_H$ and $\mu_{HM}$. Write

$$Y - \mu_H = (Y - \mu_{HM}) + (\mu_{HM} - \mu_H). \tag{A65}$$

TABLE A2. Public-data support for predictive closure and policy holonomy

| Object | Required observed support | LaDe support |
|---|---|---|
| Predictive closure | Region-date report, moments, and future target | 30,534 region-days |
| Descriptive target span | Moments, natural transition, and target loadings | 21,268 estimation rows |
| Finite policy holonomy | Four randomized orientation–mirror path cells | Zero logged assignment cells |
| Probe-response holonomy | Path cells and a common randomized terminal probe | Zero logged probe cells |

The schema assessment covers the five pinned LaDe delivery files and agrees with the source manifest and the upstream output record. The raw fields identify parcels, operational regions, cities, couriers, locations, delivery areas, acceptance events, delivery events, and dates. A finite policy-holonomy contrast requires known positive assignment probability in every orientation-by-mirror cell. Response holonomy also requires a randomized common terminal probe after endpoint measurement.

The cross term has expectation zero because $\mu_{HM} - \mu_H$ is measurable with respect to $(H, M)$ and $\mathbb{E}[Y - \mu_{HM} \mid H, M] = 0$. Squaring equation (A65), taking expectations, and subtracting the refined-information risk gives equation (75). Its right side vanishes exactly when $\mu_{HM} = \mu_H$ almost surely.

### H.2. Source and event accounting

The analysis uses the LaDe delivery files for Chongqing, Hangzhou, Jilin, Shanghai, and Yantai. The five files contain 4,514,661 rows, and timestamp parsing retains 4,514,658 rows. Three records combine an October accept time with a January delivery time in year-free timestamp strings; carrying January into the following year implies lead times of 72–89 days and a state path beyond the observed 2020 panel, so these chronology-ambiguous observations are excluded.

For parcel $i$, let $a_i$ and $d_i$ be accept and delivery timestamps. At the end of day $t$, courier backlog is

$$B_{crt} = \sum_{i \in (c,r)} \mathbf{1}\{a_i \le t + 1 < d_i\}. \tag{A66}$$

This object is computed by adding one at the accept date, subtracting one at the delivery date, and taking the courier-level cumulative sum. Aggregation gives the region identity

$$B_{rt} = B_{r,t-1} + A_{rt} - D_{rt}, \tag{A67}$$

where $A_{rt}$ and $D_{rt}$ are accepted and delivered parcels. The maximum absolute residual of (A67) is zero and every backlog is nonnegative.

Let $u_t$ denote the end-of-day clock measured in days from January 1, 2020, and write $a_i$ in the same units. The additive age moments are

$$\begin{aligned} S_{rt}^{(1)} &= u_t B_{rt} - \sum_{i \in B_{rt}} a_i, \\ S_{rt}^{(2)} &= u_t^2 B_{rt} - 2u_t \sum_{i \in B_{rt}} a_i + \sum_{i \in B_{rt}} a_i^2. \end{aligned} \tag{A68}$$

These equal $\sum_i (u_t - a_i)$ and $\sum_i (u_t - a_i)^2$. Courier-load and throughput coordinates sum squared courier counts after parcel events are aggregated to courier-day. The delivery-area coordinate first aggregates parcel counts over every raw-data chunk to region-day-area and then squares those complete counts; this order makes the result invariant to chunk size. All 4,514,658 valid parcels have a recorded delivery-area identifier. Delivery lead-time sums retain every valid parcel for throughput and backlog accounting. The reported lead-time mean and its second moment use the 4,512,857 records with lead time at most 168 hours.

The constructed data contain 242,704 courier-region-day observations and 30,534 region-day observations. Of 172 regions, 166 have at least 60 observed days. End-of-day backlog equals zero in 57.13 percent of region-days. The source city ranges differ, so every prediction split is formed within operational region.

### H.3. Prediction, matching, and rank diagnostics

For target $k$ at horizon $h$, the estimated specification is

$$\tau_{r,t+h}^k = \alpha_h^k(q_{rt}, z_{rt}) + M_{rt} B_h^k(q_{rt}) + \xi_{r,t+h}^k, \tag{A69}$$

where $q_{rt}$ is equation (73), $M_{rt}$ is equation (74), and $B_h^k$ is affine in the current report and common across conditioning cells. The conditioning vector $z_{rt}$ contains region effects, a quadratic calendar trend, weekly sine and cosine terms, current accepted flow, and exact-calendar lags of the report and accepted flow at one, two, three, and seven days. A contemporaneous-report benchmark, a history–flow benchmark, and the displayed polar model are estimated on their common complete-history sample. Ridge penalties belong to $\{0.1, 1, 10, 100, 1000, 10000\}$ and minimize average validation loss over three sequential windows: estimation through one half with validation through 0.65, estimation through 0.65 with validation through 0.80, and estimation through 0.80 with validation through the end of the outer training period. The outer evaluation set is the final 20 percent of target-observed dates within each region.

Let $L_{rt}$ be the squared-loss difference between the history–flow benchmark and the moment model on an evaluation observation. The reported mean uses every region-day observation with equal weight. Its covariance clusters the centered score two ways by region and date:

$$\widehat{\mathrm{Var}}(\bar{L}) = \frac{1}{N^2}\left[\sum_r\left(\sum_{t\in r}\widetilde{L}_{rt}\right)^2 + \sum_t\left(\sum_{r\in t}\widetilde{L}_{rt}\right)^2 - \sum_{r,t}\widetilde{L}_{rt}^2\right], \tag{A70}$$

with finite-cluster corrections on each component. This covariance targets the same observation-weighted mean as the RMSE comparison. Two-sided $t$ probabilities use $\min(G_r, G_t) - 1$ degrees of freedom, with Holm adjustments within each nine-target loss family and across the eighteen target–loss comparisons. Separate estimands weight regions and cities equally; a date-weighted record uses a seven-lag Newey–West covariance. Leave-one-city and leave-one-region calculations measure influence.

The time check uses four disjoint rolling-origin evaluation windows covering 60–70, 70–80, 80–90, and 90–100 percent of region-specific target dates, with each preceding history used for estimation and each penalty reselected inside that history. Workload sensitivities retain region-days with at least 0, 5, 10, 25, 50, 100, or 200 current parcels in backlog plus accepted flow and preserve the fixed terminal-holdout predictions. The alignment exercise permutes the fixed Gorman correction 999 times within city-date and benchmark-prediction-quartile cells. Its reference distribution requires approximate exchangeability within those cells and serves as a falsification record for correction alignment.

To move the empirical contrast toward a common input path, both learners receive realized cumulative accepted parcels between $t+1$ and $t+h$. By equation (A67), the remaining predictive difference reflects how the initial report and moments map a common realized arrival load into deliveries and terminal backlog. Realized future arrivals can respond to contemporaneous operating conditions, so this calculation remains a predictive conditioning exercise. Fixed-hyperparameter histogram gradient boosters provide an additional comparison. Since 57.13 percent of region-days have zero backlog, the absolute-loss booster predicts the sample median at zero. A two-part learner separately estimates positive-backlog probability and the conditional mean of positive log backlog, then multiplies the two components. Both nonlinear records retain the same outer split and locate the functional-form sensitivity of the phase-conditional affine specification.

The matched-history calculation standardizes 25 coordinates with training means and scales: the current report, current accepted flow, and their one-, two-, three-, and seven-day exact-calendar lags. Inside each city-date cell, it sorts all pairwise distances and greedily accepts the shortest edge whose two regions remain unused. Results are reported for the closest quartile, closest half, and complete greedy assignment.

For the descriptive transport record, current moments, next-day moments, and all nine future targets are residualized on report history, accepted flow, region effects, and calendar controls in the estimation period. With standardized residual row state $m_t$, the

TABLE A3. Backlog predictive-risk stability

| | Fixed terminal holdout | | | Rolling-origin holdouts | | |
|---|---|---|---|---|---|---|
| Horizon | Loss | Change (%) | Cluster $t$ | Loss | Change (%) | Cluster $t$ |
| 1 day | $L_2$ | 11.89 | 2.94 | $L_2$ | 3.00 | 1.84 |
| 1 day | $L_1$ | 8.83 | 6.17 | $L_1$ | 1.86 | 3.82 |
| 3 days | $L_2$ | -1.49 | -1.34 | $L_2$ | -0.71 | -1.35 |
| 3 days | $L_1$ | -0.78 | -1.77 | $L_1$ | -0.45 | -1.98 |
| 7 days | $L_2$ | 8.68 | 4.68 | $L_2$ | 1.18 | 1.74 |
| 7 days | $L_1$ | 7.18 | 10.13 | $L_1$ | 0.79 | 1.75 |

$L_2$ is squared prediction risk and $L_1$ is absolute prediction risk. Change is the percentage risk reduction from adding the six Gorman coordinates to the report-history and accepted-flow benchmark. The terminal holdout contains the final 20 percent of dates within region. Rolling-origin pools four disjoint evaluation windows. Cluster $t$ statistics use the region-and-date covariance.

fitted systems are $m_{t+1} = m_t R + e_{t+1}$ and $\tau_t = m_t B + \nu_t$. The generated loading matrix is

$$\mathcal{G}_K = [B, RB, \ldots, R^{K-1}B], \qquad K = 6. \tag{A71}$$

Its singular values and threshold ranks are descriptive functions of the observed transition. Operational regions are resampled 199 times while history–flow residualization remains fixed. This bootstrap records sampling variation in the singular spectrum conditional on that first stage. The policy-loop analogue replaces $R$ by identified holonomy maps from assigned episodes, as in theorem A4.

### H.4. Prospective assigned-loop design and power

For planning, the held-out next-day log-backlog residual from the polar predictor is centered by its city-date mean. Let $\widehat{\sigma}$ be the resulting standard deviation. In a balanced four-arm matched-set design with $N = 4B$ independent assigned clusters, the finite interaction

$$\widehat{\theta} = \frac{\overline{Y}_{+,+} - \overline{Y}_{-,+} + \overline{Y}_{+,-} - \overline{Y}_{-,-}}{4} \tag{A72}$$

has planning variance $\widehat{\sigma}^2/N$ under the independent-cell calibration. Since $\theta = \varepsilon^2\kappa_\varepsilon$, the Gaussian finite-effect threshold equals $(z_{1-\alpha/2} + z_{1-\beta})\widehat{\sigma}/\sqrt{N}$ and the curvature threshold divides this quantity by $\varepsilon^2$. The displayed finite-sample calculation replaces the size critical value by $t_{1-\alpha/2,B-1}$ and retains the Gaussian power quantile. The output includes operational-region bootstrap quantiles for $\widehat{\sigma}$ and sensitivity calculations that multiply the residual scale by 1, 1.25, 1.5, and 2. It crosses graph-retention rates 0.50, 0.75, and 1, cluster completion rates 0.70, 0.85, 0.95, and 1, path-compliance rates 0.60, 0.80, and 1, and multiplicity family sizes 1, 3, and 9. Each sensitivity cell converts retained regions and cluster completion into an integer number of complete matched sets and recomputes the Student critical value at that cell's degrees of freedom. Graph separation, buffered clusters, or an exposure mapping supplies the partial-interference partition before assignment. The planning calculation uses LaDe to estimate outcome dispersion; policy-loop assignment supplies the curvature estimand.

For the difference between two independently assigned shock-level contrasts in equation (A89), let $N_Z$ be the total number of clusters across the eight cells. The independent-cell calibration gives variance $4\widehat{\sigma}^2/N_Z$ and planning threshold

$$\text{(A73)} \qquad \mathrm{MDE}_Z = \frac{2\{t_{1-\alpha/2,B_Z-1} + z_{1-\beta}\}\widehat{\sigma}}{\sqrt{N_Z}},$$

where $B_Z = N_Z/8$ is the number of complete matched octets. The 166-region calibration supplies 160 balanced clusters and a 0.1564 log-point threshold. Preserving 41 clusters per path–shock cell uses 328 clusters and gives a 0.1066 threshold. These values concern the difference between the two shock-level contrasts. Division by $\eta_H - \eta_L$ gives the secant threshold. For symmetric levels $\eta_0 \pm \delta$, division by $2\delta$ gives the derivative threshold. If the four-arm curvature estimator has a uniform expansion $\mathbb{E}\widehat{\kappa}^{\eta}_{\varepsilon} = \kappa^{\eta} + \varepsilon^2 B(\eta) + O(\varepsilon^4)$ with $B$ continuously differentiable and $\kappa$ has three continuous environment derivatives, the centered difference has bias $O(\varepsilon^2 + \delta^2)$. Independent balanced cells give variance $O((N_Z\varepsilon^4\delta^2)^{-1})$. The stored shock-power grid uses integer matched-octet degrees of freedom at every total cluster count and reports the finite-difference numerator, from which a prespecified shock gap gives either scale.

Before assignment, a network graph built from parcel transfers, shared couriers, route overlap, and delivery-area adjacency defines graph-separated clusters and an exposure mapping. Matched sets of four use preperiod reports, Gorman moments, forecast residual scale, city, calendar block, and a forecast environmental-risk score. Within set, concealed labels assign clockwise and counterclockwise paths and their central mirrors. Each requested loop is centered on the cluster's initial report and uses a policy controller fixed before outcome realization. The primary response-holonomy protocol terminates the loop and records its endpoint before terminal-shock assignment begins. Its estimand is the finite intention-to-treat interaction in equation (A72). Exact label permutations within matched set give its randomization distribution.

For a micro-unit probe, parcel or task assignments $Z_{ic}$ are drawn after the loop endpoint is recorded and independently of path labels. Equation (A88) becomes the cluster outcome in (A72). Under Bernoulli assignment at a prespecified saturation, its randomization expectation is the average direct response under the induced peer-assignment distribution. Exposure mappings indexed by treated workload share and shared capacity report spillover sensitivity. A capacity or demand probe that changes the complete cluster receives cluster-level assignment after endpoint measurement and produces a path-by-probe factorial response with a fixed holonomy map.

The connection-comparative-static protocol assigns the environment level before path execution and holds it through the loop. A randomized capacity envelope, demand batch, or service constraint can supply this intervention. The design forms matched sets of eight, one cluster for each path–environment cell, or randomizes the two environment levels across matched four-cluster sets in separate calendar waves. The difference between the two four-arm contrasts estimates equation (A89); its gap-normalized form is a secant, and symmetric shrinking gaps estimate equation (A87). Report-loop feasibility and tracking are assessed separately within each environment. Weather, road closure, upstream flight disruption, and unanticipated local demand enter prespecified external-shock strata using preassignment forecasts; realized environment controls and shock-specific reweighting appear as sensitivity records. The confirmatory causal comparison uses randomized environment assignment.

Let $Z_b$ be the mirror-averaged orientation assignment in set $b$, let $\Delta Y_b$ be its orientation contrast in the terminal probe score, and let $\Delta A_b$ be the corresponding contrast in realized signed report area. A secondary implementation-adjusted estimand is the assignment-IV ratio

$$\widehat{\kappa}_A = \frac{B^{-1}\sum_b \Delta Y_b}{B^{-1}\sum_b \Delta A_b}. \tag{A74}$$

Its interpretation requires exclusion of path assignment from the probe response beyond realized state transport, monotonic alignment of assignment with signed area, and a common local response per realized area over the prespecified loop neighborhood. The reported quantities include the signed-area first stage and a Fieller confidence set, which remains valid when the denominator approaches zero. Endpoint report distance and maximum path tracking error are implementation outcomes. A prespecified closure tolerance defines the compliant path record while the intention-to-treat contrast retains every assigned cluster with a measured probe.

Matched-set completion requires all four path cells to produce endpoints and probe outcomes. Under independent cluster completion probability $p$, complete-set retention is $p^4$; the design table records this loss directly. The analysis supplements complete-set estimates with inverse-probability weighting from preassignment predictors and worst-case bounds over prespecified outcome support. Exposure-mapping estimates compare buffered clusters with progressively wider graph neighborhoods. The primary target family and horizons are fixed before assignment, and a randomization-based maximum statistic controls familywise size. A bridge is estimated on discovery sets, fixed, and assigned to new sets together with its reversal, an equal-cost zero-area path, and the reference state.

Two one-sided tests require the entire $1 - 2\alpha$ interval to lie inside the prespecified target margin before declaring closure.

## Appendix I. Digital-market benchmark and data construction

### I.1. Generated report paths and probe outcomes

Index the four discovery loop cells by orientation $o \in \{-1, 1\}$ and mirror $m \in \{-1, 1\}$. A fifth arm holds the report stationary. For loop scale $\varepsilon$ and periods $t = 0, \ldots, T$, the requested coordinates are

$$x_t = 0.015 m\varepsilon\{\cos(o2\pi t/T) - 1\}, \qquad y_t = 0.008 m\varepsilon \sin(o2\pi t/T). \tag{A75}$$

The mirror operation is central inversion in report coordinates. It preserves orientation and implements the signed-scale replacement $\varepsilon \mapsto -\varepsilon$ used in theorem 1. The last coordinate is set equal to the first. Interior realized reports add mean-zero tracking noise. Endpoints retain exact closure. The eight-period polygon has signed report area $o(0.000339411)\varepsilon^2$. The normalized area coordinate is $o\varepsilon^2$, with the KPI radii and polygon factor absorbed into the curvature basis. Policy coordinates are deterministic functions of the requested velocity and the generated buyer, seller, ranking, and fulfillment states, so the tables retain the path, state, and policy links used by a future controller implementation.

Let $b(c)$ denote the matched set of cluster $c$. Conditional on the public calibrations, the generated cluster-specific response to a binary terminal probe is

$$\tau_c(o, m) = \tau_0 + \xi_{b(c)} + \zeta_c + o\{\varepsilon^2\kappa + m\varepsilon^3\chi\}, \tag{A76}$$

where $\tau_0 = 0.00153237$ is the ZOZOTOWN ranking-response calibration, $\kappa = -0.000208787$, $\chi = 0.00002$, and $\xi_{b(c)}$ and $\zeta_c$ are independent centered Gaussian draws winsorized at eight standard deviations. Each component has scale 0.000025 and support $[-0.0002, 0.0002]$. Each generated user receives probe $Z_{ic} \sim \text{Bernoulli}(1/2)$. A baseline risk $p_{ic}$ is drawn from a scaled beta distribution around the ZOZOTOWN random-policy click probability 0.00418001, and

$$Y_{ic} \mid p_{ic}, Z_{ic}, c \sim \text{Bernoulli}\{p_{ic} + Z_{ic}\tau_c(o, m)\}, \tag{A77}$$

with clipping inside the unit interval. The scaled beta risk lies in $[0.00209, 0.01255]$. The support bounds on the cluster components, the discovery path term, and the bridge residuals place every generated Bernoulli probability in $[0.00209, 0.01493]$, so the clipping map is the identity under the benchmark law. The inverse-probability within-cluster

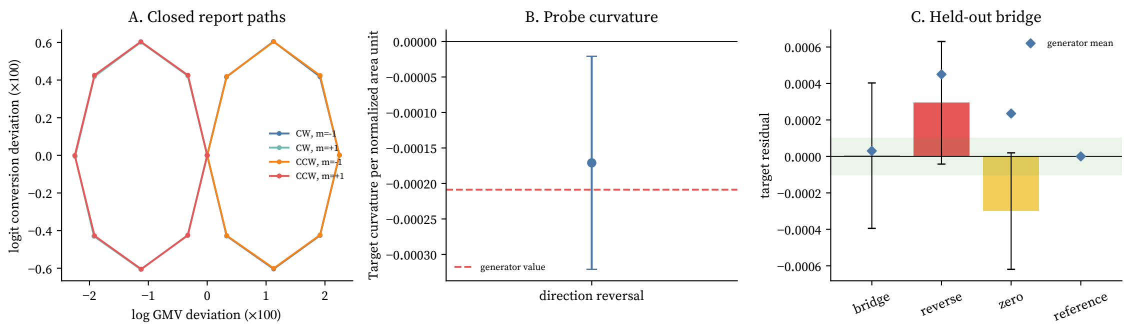


FIGURE A2. Direction reversal and bridge validation in the constructed platform benchmark

Panel A gives the realized mean report paths for four orientation-by-mirror arms. Panel B compares the direction-reversal curvature estimate and its 95-percent interval with the generator value. Panel C reports probe-effect residuals relative to the reference-state arm in 80 held-out clusters; diamonds give generator means and bars give sample estimates with 95-percent intervals. The shaded region is the prespecified bridge margin. All paths, probes, and outcomes are researcher generated.

probe score estimates $\tau_c$, and the reported benchmark fixes the covariate-adjustment slope at zero before analysis. Substituting equation (A76) into the four-arm contrast gives $\mathbb{E}[\widehat{\kappa}] = \kappa$ because mirror averaging removes $\chi$ and randomized labels balance the centered cluster component. The constant symmetric curvature across loop sizes follows from this generator equation. Report tracking noise is retained in the path tables and remains outside the generated terminal target equation.

The bridge wave draws fresh clusters and uses

$$\tau_c(a) = \tau_0 + \xi_{b(c)} + \zeta_c + r_a, \tag{A78}$$

for bridge arm $a$. The configured residuals are 0.000030 for the baseline bridge, 0.000450 for its reversal, 0.000235 for an equal-cost zero-area path, and zero for the reference state. Discovery and bridge assignments are randomized independently within their matched sets. The matched-set component $\xi_{b(c)}$ cancels from the within-set contrasts in equation (A92); the cluster component and terminal Bernoulli sampling remain in their sampling variance.

The held-out bridge point estimate is $4.00 \times 10^{-6}$, inside the prespecified $10^{-4}$ target margin. Its 90-percent equivalence interval is $[-3.48, 3.56] \times 10^{-4}$, and the TOST $p$ value is 0.321. The generated wave therefore resolves the bridge point estimate while leaving the prespecified equivalence claim statistically open. The direction-reversal curvature estimate is $-1.71 \times 10^{-4}$ with matched-set standard error $7.66 \times 10^{-5}$ and randomization $p = 0.014$. The realized-area IV ratio is $-0.503$, its signed-area first-stage $t$ statistic is 543, and its Fieller interval is $[-0.964, -0.042]$ in target-response units per unit of realized report area.

TABLE A4. Constructed platform benchmark

| Object | Estimate | Standard error | Reference |
|---|---|---|---|
| Direction-reversal curvature | -0.000171 | 0.000077 | -0.000209 |
| Stationary probe effect | 0.001591 | 0.000074 | 0.001532 |
| Held-out bridge residual | 0.000004 | 0.000203 | 0.000030 |

Estimates use generated contract data. Curvature is measured per normalized loop-area coefficient $\varepsilon^2$; the GMV and conversion radii and the eight-period polygon factor are absorbed into the area basis. Bridge units are changes in the terminal purchase-probability response.

### I.2. Calibration and robustness diagnostics

The conversion of 3,406,115 MerRec events gives 320,180 buyer-week observations and 2,592 cohort-week observations. The final four weeks are held out from transition fitting. In the temporal pseudo-target exercise, May through August form the source period, September is the calibration period, and October is the evaluation period. The domain-classifier AUC is 0.828, and clipped density-ratio weights retain effective sample share 0.287. These diagnostics govern the field replacement and play no role in defining the generated curvature.

The eBay calculation streams 98,307,281 listing rows and 47,377,200 bargaining rows. Four deterministic residue classes modulo 200 contain between 6,250 and 6,326 sellers. Their held-out standardized RMSE lies between 0.5890 and 0.5946, and their transition spectral radius lies between 0.9863 and 0.9915. The ZOZOTOWN calculation streams 26,892,285 impressions, with campaign-position randomized effects ranging from 0.001197 to 0.001865. The KuaiRand calculation processes 4,481,469 eligible interactions and reports carryover estimates over 30-, 60-, and 120-minute linkage windows together with the placebo range. The Amazon record links 6,112 routes to observed sequences and packages. Station and date fixed effects explain 0.0766 of the route-quality index variation; these associations supply state support.

Let $\eta_S$ collect the source calibrations and let $P^B_{\eta_S}$ denote the declared benchmark law. A field platform has transition parameter $\eta_0$ and target moment $g_0(\eta_0) = 0$.

PROPOSITION A2 (Calibration and target separation). *Conditional on $P^B_{\eta_S}$, randomized path and probe assignments identify the benchmark target holonomy and bridge residual. For field data as $n_0 \to \infty$, choose a compact neighborhood $\mathcal{N}_0$ with $\eta_0 \in \operatorname{int}(\mathcal{N}_0)$ and let $\widehat{\eta}_\lambda$ be a consistent minimizer of the criterion below. Suppose $\sqrt{n_0}\widehat{g}_0(\eta_0)$ is asymptotically linear and $\partial_\eta \widehat{g}_0(\eta)$ converges uniformly on a neighborhood of $\eta_0$ to a continuous matrix function $G(\eta)$. Let $G_0 = G(\eta_0)$ have full column rank, let $W_0$ be symmetric positive definite, suppose $V_S^{-1}$ is symmetric positive semidefinite with $\|V_S^{-1}\|_{\mathrm{op}} = O_p(1)$, and suppose $\widehat{\eta}_S = O_p(1)$. The target-*

*anchored estimator*

(A79)

$$\widehat{\eta}_\lambda \in \arg\min_{\eta\in\mathcal{N}_0}\left\{n_0\widehat{g}_0(\eta)'W_0\widehat{g}_0(\eta)+\lambda_{n_0}(\eta-\widehat{\eta}_S)'V_S^{-1}(\eta-\widehat{\eta}_S)\right\},\qquad \lambda_{n_0}\geq 0,\quad \frac{\lambda_{n_0}}{\sqrt{n_0}}\to 0,$$

*satisfies*

$$\sqrt{n_0}(\widehat{\eta}_\lambda-\eta_0)=-(G_0'W_0G_0)^{-1}G_0'W_0\sqrt{n_0}\widehat{g}_0(\eta_0)+o_p(1) \tag{A80}$$

*for every fixed source–target parameter difference. Point transport of a source transition block requires measurement alignment, conditional transition invariance, overlap, and rank for that block.*

### I.3. Proof of proposition A2

Conditional on the benchmark configuration, path labels are randomized within matched sets and the terminal probe is randomized within cluster. Iterated expectations of the inverse-probability probe score therefore give $\tau_c(a)$, and averaging with the assigned path weights gives the benchmark finite-loop, curvature, and bridge estimands.

For the field statement, consistency and interiority make the first-order condition of equation (A79) hold with probability approaching one. Write $\widehat{G}_n(\eta)=\partial_\eta\widehat{g}_0(\eta)$ and $\overline{G}_n=\int_0^1\widehat{G}_n\{\eta_0+t(\widehat{\eta}_\lambda-\eta_0)\}\,dt$. The integral mean-value expansion gives $\widehat{g}_0(\widehat{\eta}_\lambda)=\widehat{g}_0(\eta_0)+\overline{G}_n(\widehat{\eta}_\lambda-\eta_0)$, while uniform derivative convergence and consistency give $\widehat{G}_n(\widehat{\eta}_\lambda)\to_p G_0$ and $\overline{G}_n\to_p G_0$. After division by $2\sqrt{n_0}$, the first-order condition is

$$0=\widehat{G}_n(\widehat{\eta}_\lambda)'W_0\left\{\sqrt{n_0}\widehat{g}_0(\eta_0)+\overline{G}_n\sqrt{n_0}(\widehat{\eta}_\lambda-\eta_0)\right\}+\frac{\lambda_{n_0}}{\sqrt{n_0}}V_S^{-1}(\widehat{\eta}_\lambda-\widehat{\eta}_S). \tag{A81}$$

The coefficient on $\sqrt{n_0}(\widehat{\eta}_\lambda-\eta_0)$ converges to $G_0'W_0G_0$, while the portion of the penalty multiplying this scaled difference has coefficient $\lambda_{n_0}/n_0=o(1)$ and the remaining penalty term is $o_p(1)$. Full column rank of $G_0$ and positive definiteness of $W_0$ make $G_0'W_0G_0$ invertible. Solving (A81) first gives $\sqrt{n_0}(\widehat{\eta}_\lambda-\eta_0)=O_p(1)$ and then gives equation (A80). The expansion permits a fixed difference between $\eta_S$ and $\eta_0$.

For point transport of a selected source block, let $V$ denote aligned state and transport covariates and let $r(v)=dP_0^V(v)/dP_S^V(v)$. Conditional transition invariance and overlap give

$$\mathbb{E}_S[r(V)\psi(X^+,V;\eta_0)]=\int\mathbb{E}_0[\psi(X^+,v;\eta_0)\mid V=v]dP_0^V(v)=g_0(\eta_0)=0. \tag{A82}$$

The block rank condition gives local identification. Failure of a point-transport condition sends the source coefficient to the target-anchored penalty or a sensitivity set.

### I.4. Target and coordinate-block comparisons

Backlog-age, courier-distribution, and delivery-area/service blocks reduce benchmark RMSE by 5.59, 6.75, and 6.43 percent, respectively. Seven-day backlog RMSE falls 4.44 percent and absolute risk falls 7.18 percent, while the three-day measures change by −0.74 and −0.78 percent. Throughput RMSE changes are −0.69, −0.22, and 0.72 percent; lead-time changes are −15.96, −0.60, and −0.14 percent. The variation across outcomes and horizons follows the target dependence of $\mathcal{W}^{\star}_{\tau,s}$.

## Appendix J. Implementation, environment, and finite-loop extensions

### J.1. A connection on policy-path space

In a forward-looking equilibrium, current policy is linked to the entire report path. Fix an initial state and a terminal condition, choose a local chart for each reported date, and stack $T$ policy vectors as $U \in \mathbb{R}^{kT}$. Let $\Phi_T(U; s_0) \in \mathbb{R}^{mT}$ denote the resulting equilibrium report path, with the stacked coordinates carrying the product phase metric. A requested path $\gamma \in \mathbb{R}^{mT}$ is locally feasible at $U_0$ when $\gamma - \Phi_T(U_0; s_0)$ belongs to the range of $D_U\Phi_T(U_0; s_0)$. Given a positive-definite path cost $\mathsf{R}_T$, the linearized lift is

$$\Delta U^H = \mathsf{R}_T^{-1} D\Phi_T' \big(D\Phi_T \mathsf{R}_T^{-1} D\Phi_T'\big)^{\dagger} \big(\gamma - \Phi_T(U_0; s_0)\big). \tag{A83}$$

PROPOSITION A3 (Path-space policy connection). *Suppose $\Phi_T$ is $C^1$ and $D_U\Phi_T$ has constant rank $\rho_T$ near $U_0$. Equation* (A83) *is the minimum-$\mathsf{R}_T$-norm solution of the linearized path restriction. If $\rho_T = mT$, the exact solution set $\{U : \Phi_T(U; s_0) = \gamma\}$ is a local manifold of dimension $kT - mT$ around each nearby solution, and the Newton update based on* (A83) *is locally defined. If $\rho_T < mT$, the same expression lifts the attainable projection of the requested path and leaves an orthogonal feasibility residual.*

The path-space map imposes expectations, market clearing, and terminal conditions before it is differentiated. Its derivative therefore supplies the policy connection for a perfect-foresight or sequence-space implementation. Singular values recomputed along the Newton iterates show whether the solution remains in the same regular stratum and how well conditioned the requested loop is.

### J.2. Exogenous environments and comparative statics

Let the scalar $\eta$ index an exogenous environment such as demand intensity, weather severity, input cost, or available capacity. Keep the report map $q$ fixed and allow $(f^\eta, G^\eta, R^\eta, \tau^\eta)$, the attainable distribution $\mathcal{E}^\eta$, and its lift $L^{E,\eta}$ to vary smoothly with $\eta$. Fix a report loop $\gamma$ that remains feasible on a neighborhood of $\eta_0$ and define

$$\mathsf{b}_t^\eta(z) = f_z^\eta + L_z^{E,\eta}\big(\dot\gamma_t - d^\eta_{\gamma(t)}\big), \qquad \dot S_t^\eta = \mathsf{b}_t^\eta(S_t^\eta), \qquad S_0^\eta = s_\eta^\circ. \tag{A84}$$

The endpoint is $\mathrm{Hol}_\gamma^\eta(s_\eta^\circ) = S_1^\eta$, and the shock-indexed target defect is $h_\tau^\eta(\gamma, s_\eta^\circ) = \tau^\eta(S_1^\eta) - \tau^\eta(s_\eta^\circ)$. The baseline $s_\eta^\circ$ may be a shock-specific stationary state or a common initial state.

PROPOSITION A4 (Shock-indexed holonomy comparative statics). *Suppose* $\mathrm{b}_t^\eta$ *is continuously differentiable in* $(z,\eta)$, $\tau^\eta$ *and* $s_\eta^\circ$ *are continuously differentiable in* $\eta$, *and the lifted solutions remain in a common compact regularity neighborhood. Then* $J_t^\eta = \partial_\eta S_t^\eta$ *solves*

$$\dot{J}_t^\eta = D_s \mathrm{b}_t^\eta(S_t^\eta) J_t^\eta + \partial_\eta \mathrm{b}_t^\eta(S_t^\eta), \qquad J_0^\eta = \partial_\eta s_\eta^\circ, \tag{A85}$$

*and*

$$\begin{aligned} \frac{d}{d\eta} h_\tau^\eta(\gamma, s_\eta^\circ) = {} & \partial_\eta \tau^\eta(S_1^\eta) + D_s \tau^\eta(S_1^\eta) J_1^\eta \\ & - \partial_\eta \tau^\eta(s_\eta^\circ) - D_s \tau^\eta(s_\eta^\circ) \partial_\eta s_\eta^\circ. \end{aligned} \tag{A86}$$

*At a fixed base state and fixed phase directions,* $\kappa_\tau^\eta = D_s \tau^\eta \Omega^\eta$ *satisfies* $\partial_\eta \kappa_\tau^\eta = D_s(\partial_\eta \tau^\eta)\Omega^\eta + D_s \tau^\eta \partial_\eta \Omega^\eta$.

Equation (A86) separates a direct change in the probe mapping from the change in state transported by the shock-indexed policy connection. For a stochastic innovation path, the equation applies conditionally on the realized path. Integrating over a prespecified law gives the regime-specific expected defect, and a path experiment balances this law across orientation arms through randomization within calendar and forecast blocks. Two fixed shock levels identify a finite change; dividing by their intensity gap gives a secant. With symmetric levels $\eta_0 \pm \delta$, the derivative estimator is

$$\widehat{\partial_\eta \kappa}_{\varepsilon,\delta} = \frac{\widehat{\kappa}_\varepsilon^{\eta_0+\delta} - \widehat{\kappa}_\varepsilon^{\eta_0-\delta}}{2\delta}. \tag{A87}$$

Under a symmetric four-arm path design at each shock level, uniform fourth-order path expansions, three derivatives in $\eta$, and balanced independent clusters, its bias is $O(\varepsilon^2 + \delta^2)$ and its variance is $O((J\varepsilon^4\delta^2)^{-1})$. Estimating an infinitesimal comparative static therefore requires both the path and shock increments to shrink. A fixed pair of shock levels instead yields the corresponding finite change.

### J.3. Randomized shocks and response holonomy

Shock timing distinguishes two estimands. The first asks whether the completed path changes the response to a common terminal probe. Cluster $c$ completes assigned path $a$, after which eligible terminal micro units receive shock level $Z_{ic} \in \{0,1\}$ with prespecified probability $p_c$. At a fixed saturation and exposure mapping, the Horvitz–Thompson response score

$$\overline{R}_c(a) = \frac{1}{M_c} \sum_{i=1}^{M_c} \left( \frac{Z_{ic} Y_{ic}}{p_c} - \frac{(1 - Z_{ic}) Y_{ic}}{1 - p_c} \right) \tag{A88}$$

identifies the cluster response to the assigned demand, priority, or capacity probe under its randomization design. Substituting $\overline{R}_c(a)$ for $\overline{Y}_c^p(a)$ in equation (26) identifies the target curvature of the shock response $\tau^R(s) = \mathbb{E}[Y(1) - Y(0) \mid S = s]$. This estimand compares the causal response to the same terminal shock after opposite report loops. Because shock assignment begins after the path endpoint is recorded, the endpoint map $\mathrm{Hol}_\gamma$ is held fixed and the contrast isolates the probe-response channel.

The second estimand is the connection comparative static in Proposition A4. Here the environment is assigned before the path and maintained while the path is executed. A randomized capacity envelope, exogenous demand batch, or service constraint can then change both the lifted dynamics and the endpoint map $\mathrm{Hol}^{\eta}_{\gamma}$. Crossing two environment levels with the orientation-by-mirror assignment gives eight cells and the finite-change estimand

$$\Delta_Z \kappa_\varepsilon = \kappa_\varepsilon^{(1)} - \kappa_\varepsilon^{(0)}, \tag{A89}$$

where each $\kappa_\varepsilon^{(z)}$ is a four-arm contrast within environment level $z$. Orthogonal path and environment assignments identify (A89). Dividing by the prespecified environment gap gives a secant. With symmetric levels $\eta_0 \pm \delta$, division by $2\delta$ gives equation (A87). A cluster-level shock applied after the path yields the same factorial algebra, now with a probe-intensity interpretation and a fixed endpoint map. Weather, upstream flight disruption, and local demand innovations can index observational regimes when their conditional assignment law is justified. In a field design, randomization blocks use preassignment forecasts and calendar waves; realized postassignment environment variables are reserved for reported regime definitions and sensitivity analyses.

THEOREM A1 (Joint shrinking-path and environment inference). *Let $\varepsilon = \varepsilon_J \to 0$ and $\delta = \delta_J \to 0$. Suppose independent clusters are randomized across the eight cells $(o, \sigma, z) \in \{+, -\}^3$ with limiting cell shares $\pi_{o,\sigma,z} \in (0, 1)$, uniformly bounded $2 + \nu$ moments, and covariance limits $\Sigma_{o,\sigma,z}$. Suppose uniformly near $\eta_0$,*

$$\mathbb{E}\widehat{\kappa}^{\eta}_\varepsilon = \kappa^{\eta} + \varepsilon^2 B(\eta) + r_\varepsilon(\eta), \qquad \sup_{\eta} \|\partial_\eta r_\varepsilon(\eta)\| = O(\varepsilon^4), \tag{A90}$$

*where $B$ has a bounded derivative and $\kappa^{\eta}$ has a bounded third derivative. Then the estimator in equation* (A87) *has bias $O(\varepsilon^2 + \delta^2)$ and*

$$\sqrt{J}\varepsilon^2\delta\left(\widehat{\partial_\eta \kappa}_{\varepsilon,\delta} - \mathbb{E}\widehat{\partial_\eta \kappa}_{\varepsilon,\delta}\right) \Longrightarrow \mathcal{N}(0, V_\eta), \qquad V_\eta = \frac{1}{64}\sum_{o,\sigma,z} \frac{\Sigma_{o,\sigma,z}}{\pi_{o,\sigma,z}}. \tag{A91}$$

*Consistency follows when $J\varepsilon^4\delta^2 \to \infty$. Centering at $\partial_\eta \kappa^{\eta_0}$ additionally follows when $\sqrt{J}\varepsilon^2\delta(\varepsilon^2 + \delta^2) \to 0$.*

For the digital benchmark, each matched set contains one cluster from every arm. Let $b = 1, \ldots, B$ index independent matched sets and let $\overline{Y}^{p}_{b,o,\sigma}$ be the cluster probe mean in its assigned cell. Define

$$D_b(\varepsilon) = \frac{\overline{Y}^{p}_{b,+,+} - \overline{Y}^{p}_{b,-,+} + \overline{Y}^{p}_{b,+,-} - \overline{Y}^{p}_{b,-,-}}{4\varepsilon^2}, \qquad \kappa^{\mathrm{MS}}_\varepsilon = \mathbb{E}[D_b(\varepsilon)], \qquad \widehat{\kappa}^{\mathrm{MS}}_\varepsilon = \frac{1}{B}\sum_{b=1}^{B} D_b(\varepsilon). \tag{A92}$$

THEOREM A2 (Matched-set path inference). *Fix $\varepsilon > 0$. Suppose the matched sets are independently and identically sampled, every set assigns one cluster to each of the four loop cells, path labels are randomized within set, and $\mathbb{E}\|D_b(\varepsilon)\|^{2+\delta} < \infty$. Dependence among the four clusters inside a set is unrestricted. As*

*$B \to \infty$, $\widehat{\kappa}_\varepsilon^{\mathrm{MS}}$ identifies the average set-level four-arm contrast and*

$$\text{(A93)} \qquad \sqrt{B}\left(\widehat{\kappa}_\varepsilon^{\mathrm{MS}} - \kappa_\varepsilon^{\mathrm{MS}}\right) \Longrightarrow \mathcal{N}\big(0, \mathrm{Var}[D_b(\varepsilon)]\big).$$

*The sample variance of $D_b(\varepsilon)$ divided by $B$ estimates the variance of $\widehat{\kappa}_\varepsilon^{\mathrm{MS}}$. Under a sharp null, randomization inference permutes the four path labels within each set.*

Squared bias is $O(\varepsilon^4)$ and variance is $O((n\varepsilon^4)^{-1})$. When both leading constants are positive, balancing them gives $\varepsilon \asymp n^{-1/8}$ and root mean squared error of order $n^{-1/4}$. Confidence intervals centered on the limiting curvature use an undersmoothing sequence within the interval in Theorem 2. When $\kappa_\varepsilon = \kappa + c\varepsilon^2 + o(\varepsilon^2)$ uniformly, two loop sizes identify a Richardson extrapolation; its joint arm covariance enters the confidence interval.

### J.4. Holonomy-invariant polar quotients

The polar form in (54) decodes a target at one state. Prediction after loop concatenation also requires an evolution law for the moments. Consider a finite distribution and let $H \in \mathbb{K}^{N\times h}$ contain the constant and phase-known loadings. Let $P_1, \dots, P_J$ be a library of linear policy holonomies that map the relevant distribution domain into itself and satisfy $P_j H = H$, so every map preserves the phase report $\mu H$. A $g$-coordinate polar quotient consists of $W$, $B$, $C$, and matrices $(A_j, R_j)$ satisfying

$$\text{(A94)} \qquad D = HC + WB, \qquad P_j W = HA_j + WR_j, \qquad j = 1, \dots, J.$$

Writing $h_x = \mu H$ and $m = \mu W$, these equations give

$$\text{(A95)} \qquad \tau(\mu) = h_x C + mB, \qquad m(\mu P_j) = h_x A_j + mR_j.$$

The first equation is a Gorman-form target aggregator. The second makes the additive coordinates an affine state representation of policy holonomy.

Let $\pi : \mathbb{K}^N \to \mathbb{K}^N/\operatorname{col}(H)$ be the quotient map and let $\overline{P}_j$ denote the map induced by $P_j$. Define

$$\text{(A96)} \qquad \overline{\mathcal{V}}_\infty = \operatorname{span}\left\{\overline{P}_{i_k}\cdots\overline{P}_{i_1}\pi(Dc) : k \geq 0,\ i_\ell \in \{1, \dots, J\},\ c \in \mathbb{K}^r\right\}, \qquad d_G = \dim \overline{\mathcal{V}}_\infty.$$

Theorem A3 (Holonomy-polar aggregation). *The minimum number of additive coordinates in* (A94) *equals $d_G$. A quotient attaining $d_G$ is obtained by lifting a basis of $\overline{\mathcal{V}}_\infty$ to the columns of $W$. The iteration*

$$\text{(A97)} \qquad \overline{\mathcal{V}}_0 = \operatorname{span}\pi(\operatorname{col} D), \qquad \overline{\mathcal{V}}_{\ell+1} = \overline{\mathcal{V}}_\ell + \sum_{j=1}^{J} \overline{P}_j \overline{\mathcal{V}}_\ell$$

*reaches $\overline{\mathcal{V}}_\infty$ after at most $N - \operatorname{rank}(H)$ strict enlargements.*

Corollary A1 (Additive realization of the dynamic target quotient). *In the finite linear setting of theorem A3, let $U$ be a relative-open subset of the relative interior of a phase fiber, so its tangent space is $\mathcal{T}_H = \{z \in \mathbb{K}^N : zH = 0\}$. Let $g_j(\mu) = \mu P_j$ and let $\tau(\mu) = \mu D$. The response codistribution in* (68), *restricted to $\mathcal{T}_H$, has rank $d_G$. The matrix $W$ constructed in theorem A3 realizes $M^\star(\mu) = \mu W$ with additive microstate coordinates. Every linear additive representation that propagates the target through the loop library has at least $d_G$ coordinates.*

The target kernel and policy-loop library therefore produce a finite subspace algorithm. Exact linear aggregation has $d_G = 1$ when a common Gorman coordinate spans the generated subspace. Larger values count the additional additive statistics needed to carry the target through policy history. This construction is related to finite-state lumpability (Buchholz 1994). Here a specified counterfactual kernel generates the quotient, and the transition maps are policy holonomies based on the phase diagram.

COROLLARY A2 (Finite-cycle polar closure). *For one loop with $m^+ = h_x A + mR$, the k-cycle moment and target defects are*

$$m_k = m_0 R^k + h_x A \sum_{\ell=0}^{k-1} R^\ell, \qquad \tau(\mu P^k) - \tau(\mu) = \left[ m_0 (R^k - I_g) + h_x A \sum_{\ell=0}^{k-1} R^\ell \right] B. \tag{A98}$$

*The target closes after k cycles exactly when the bracketed vector belongs to the right kernel of B. The two identities $R^k = I_g$ and $A \sum_{\ell=0}^{k-1} R^\ell = 0$ give state-independent closure on the polar quotient.*

Equation (A98) gives the economic counterpart of finite-cycle closure for a trajectoid. The phase point returns after every traversal, while the affine matrix $R$ transports the hidden aggregate orientation. The accumulated translation determines the cycle count at which the target also returns.

### J.5. Finite-loop polar transport inference

Let $\gamma = (j_1, \ldots, j_T)$ be a word in the loop library, with every loop based at the same phase point. Define

$$R_\gamma = R_{j_1} \cdots R_{j_T}, \qquad a_\gamma = \sum_{t=1}^{T} A_{j_t} R_{j_{t+1}} \cdots R_{j_T}, \tag{A99}$$

where the empty matrix product is $I_g$. Repeated use of (A95) gives

$$m_T = m_0 R_\gamma + h_x a_\gamma, \qquad h_\tau(\gamma) = \left[ m_0 (R_\gamma - I_g) + h_x a_\gamma \right] B. \tag{A100}$$

The coefficients can be estimated from target-sensitive moments without observing the full distribution vector. For loop type $j$, let episode $i$ supply the phase-known row $h_{ij}$, the target-sensitive moments $m_{ij}$ and $m^+_{ij}$ before and after the loop, and a probe target $\tau_{ij}$. Write $z_{ij} = (h_{ij}, m_{ij})$ and

$$m^+_{ij} = z_{ij} \Theta_j + \eta_{ij}, \qquad \Theta_j = \begin{bmatrix} A_j \\ R_j \end{bmatrix}, \qquad \tau_{ij} = h_{ij} C + m_{ij} B + \nu_{ij}. \tag{A101}$$

THEOREM A4 (Polar transport identification and inference). *Let n denote the number of independently sampled episode clusters. Suppose the regression errors in* (A101) *have conditional mean zero and the cluster score vectors have uniformly bounded* $2 + \delta$ *moments. Suppose every loop type has a limiting episode share in* $(0, 1)$*, the loop-type sample second moments converge in probability to positive-definite matrices* $Q_j = \mathbb{E}[z'_{ij} z_{ij} \mid j]$*, and the target-regression sample second moment converges to its positive-definite population counterpart. Suppose the stacked cluster scores satisfy the Lindeberg condition and* *their covariance matrices converge to a finite matrix $\Omega$. Any estimated initial moments entering the plug-in target are assumed to have a joint asymptotically linear representation in the same cluster array; fixed initial moments satisfy this condition with a zero influence term. Then $(A_j, R_j)_{j=1}^{J}$, $B$, and $C$ are identified by the population regressions, and their least-squares estimators are jointly asymptotically linear as $n \to \infty$. For every fixed loop word $\gamma$, the plug-in estimator obtained from* (A100) *satisfies*

$$\sqrt{n}\left(\widehat{h}_\tau(\gamma) - h_\tau(\gamma)\right) \Longrightarrow \mathcal{N}(0, J_\gamma \Sigma J_\gamma'), \tag{A102}$$

*where $\Sigma$ is the joint cluster covariance of the coefficient and initial-moment estimators and $J_\gamma$ is the Jacobian of* (A100). *An estimated or cross-fitted measurement matrix $W$ enters* (A102) *when its estimator has a joint asymptotically linear representation with an $o_p(n^{-1/2})$ remainder; its influence term is appended to $\Sigma$.*

The transport estimator targets the finite-loop defect in (A100). Its normalization uses matrix products and a common slope. The direct curvature estimator instead scales a randomized arm contrast by $\varepsilon^2$. Direction reversal identifies the local geometric derivative, while polar transport predicts finite policy cycles from a loop-stable aggregate state law. Comparing their implications across feasible loop sizes provides a specification check for the quotient.

## References


**Ambrose, Warren and Isadore M. Singer**, "A Theorem on Holonomy," *Transactions of the American Mathematical Society*, 1953, *75* (3), 428–443.

**Buchholz, Peter**, "Exact and Ordinary Lumpability in Finite Markov Chains," *Journal of Applied Probability*, 1994, *31* (1), 59–75.

**Hirsch, Morris W.**, *Differential Topology*, Vol. 33 of *Graduate Texts in Mathematics*, New York: Springer, 1976.